Multi-Objective Optimization and Analysis of Bottom Purged Steelmaking ladles

BY

BIRANJAY KUMAR

B.TECH (MECHANICAL ENGINEERING), 2020

G.B.PANT ENGINEERING COLLEGE GHURDAURI, PAURI

EXAMINATION ROLL NO. - M4PRD24001B

THESIS

SUBMITTED IN PARTIAL FULLFILLMENT OF THE REQUIREMENTS FOR THE AWARD OF THE DEGREE OF MASTER OF PRODUCTION ENGINEERING IN THE FACULTY OF ENGINEERING AND TECHNOLOGY

JADAVPUR UNIVERSITY

2024

DEPARTMENT OF PRODUCTION ENGINEERING

JADAVPUR UNIVERSITY

KOLKATA – 700032

INDIA

JADAVPUR UNIVERSITY

FACULTY OF ENGINEERING AND TECHNOLOGY

DATE-

CERTIFICATE OF RECOMMENDATION

I HEREBY RECOMMEND THAT THE THESIS ENTITLED **"MULTI-OBJECTIVE OPTIMIZATION AND ANALYSIS OF BOTTOM PURGED STEELMAKING LADLES"** CARRIED OUT UNDER MY/OUR GUIDANCE BY **MR. BIRANJAY KUMAR** MAY BE ACCEPTED IN THE PARTIAL FULFILLMENT OF THE REQUIREMENTS FOR THE DEGREE OF **"MASTER OF PRODUCTION ENGINEERING".**

COUNTER SIGNED BY-

……..	……..
HEAD,	**DEAN,**
Dept. of Production Engineering	Faculty of Engg. & Technology
Jadavpur university	Jadavpur University
Kolkata-700032	Kolkata- 700032

THESIS ADVISORS-

……	……
Prof. Arunanshu Shekhar Kuar	**Dr. Asim Gopal Barman**
PROFESSOR	**ASSOCIATE PROFESSOR**
Dept. of Production Engineering	Dept. of Production Engineering
Jadavpur University	Jadavpur university
Kolkata- 700032	Kolkata- 700032

JADAVPUR UNIVERSITY

FACULTY OF ENGINEERING & TECHNOLOGY

CERTIFICATE OF APPROVAL

The foregoing thesis is hereby approved as a creditable study of an engineering subject carried out and presented in a manner satisfactory to warrant its acceptance as a prerequisite to the degree for which it has been submitted. It is understood that by this approval, the undersigned do not necessarily endorse or approve any statement made, opinion expressed and conclusion drawn therein but thesis only for the purpose for which it has been submitted.

COMMITTEE ON FINAL EXAMINATION FOR

EVALUATION OF THE THESIS ……

(External Examiner)

…….

(Internal Examiners)

ACKNOWLEDGEMENT

I would like to express my profound gratitude and thanks to my project guide Prof. Arunanshu Shekhar Kuar and Dr. Asim Gopal Barman, Department of Production Engineering, Jadavpur University, Kolkata for introducing the present topic and intellectual support, inspiring guidance and his invaluable encouragement, suggestions and cooperation helps a lot to completion of my project work successfully.

I am also thankful to Prof. Bijoy Bhattacharyya, Former Head of Department, Production Engineering, Jadavpur University, Kolkata, for providing necessary information and guidance regarding the project. I would like to express my warmest gratitude to Prof. Bijan Sarkar, Head of Department, Production Engineering, Jadavpur University, Kolkata, for providing great support and guidance regarding the thesis. I am thankful to all respected professors and teachers of the department of Production Engineering who took keen interest in the work and gave their valuable suggestions.

I would like to thank Jadavpur University for providing me this wonderful opportunity and all my friends for their kind cooperation which helps me to complete my project.

I feel pleased and privileged to fulfil my parents' ambition, and I am greatly indebted to them for bearing the inconvenience during my M.Prod.E course. Thank you, my beloved parents.

……

(BIRANJAY KUMAR)

ABSTRACT

During secondary steelmaking operations, argon gas is introduced into steelmaking ladles to speed up mass and heat transmission in the melt. Additionally, slag eye development and wall shear stresses are caused by ladle hydrodynamics, which lowers the quality of the steel.

A mathematical model is developed in this study to forecast the wall shear stress, slag opening area, and mixing time in single and dual bottom purged industrial steelmaking ladles.

To estimate the same, dimensional less empirical correlations have also been suggested. Further to minimize the objective functions i.e., mixing time, slag opening area, and wall shear stress, some multi-objective optimization techniques based on evolutionary algorithms have been introduced.

Because the objective functions were opposing in nature, a Pareto optimum solution set—which included simultaneous optimal solutions is produced. Additionally, the ideal process parameters for the ladle's best performance were determined. Further an analysis is done using ANSYS software.

TABLE OF CONTENT **Page no.**

LIST OF FIGURES

LIST OF TABLES

LIST OF SYMBOLS

g	Acceleration due to gravity, m s^{-2}
v	Velocity, m s^{-1}
A_s	Slag opening area, m^2
D_ω	Cross diffusion term
G	Generation or production
H	Metal bath height, m
h	Initial slag layer thickness, m
I	Turbulent intensity, %
i	Phase index
k	Turbulent kinetic energy, m^2s^{-2}
l	turbulent length scale, m
m	Mass fraction of tracer
P	Pressure, Pa
Q	Total gas flow rate, m^3s^{-1}
R	Radius of the base of the ladle, m
$R1$	Distance of gas inlet-1 from the base centre, m
$R2$	Distance of gas inlet-2 from the base centre, m
$R3$	Distance between the two gas inlets, m
S	Strain rate tensor, s^{-1}
S_{ct}	Turbulent Schmidt number
t	Time, s
t_{mix}	95% Bulk mixing time, s
Y	Dissipation due to turbulence
α	Volume fraction
k	Interface curvature, m^{-1}
μ	Dynamic viscosity, kg $m^{-1}s^{-1}$
μ_t	Turbulent viscosity, kg $m^{-1}s^{-1}$
ω	Specific dissipation rate, s^{-1}
ρ	Density, kg m^{-3}
ρ_{st}	Density of steel, kg m^{-3}
σ	Surface tension, N m^{-1}
τ	Wall shear stress, Pa
τ_{max}	Maximum wall shear stress, Pa
θ	Angle between the two gas inlets,

1. Introduction

In the secondary metallurgy of steel making, gas stirring is extensively employed to attain a homogenous distribution of alloying elements and temperature of bath. It is employed for the process of deoxidation, desulphurisation and removal of inclusions and it intensifies the rate of reactions. Argon gas is injected through a nozzle located at the bottom of the ladle and this breaks up and forms gas bubbles. The rising bubbles tends to move upwards, forming a turbulent plume, and subsequently, a circulatory movement of the steel within the ladle. This reduces the time required to homogenize the chemical composition of alloying elements and the temperature. Meanwhile at sufficiently high flow rates, the bubbles moving upwards break the slag layer forming an open-eye as shown in figure 1.

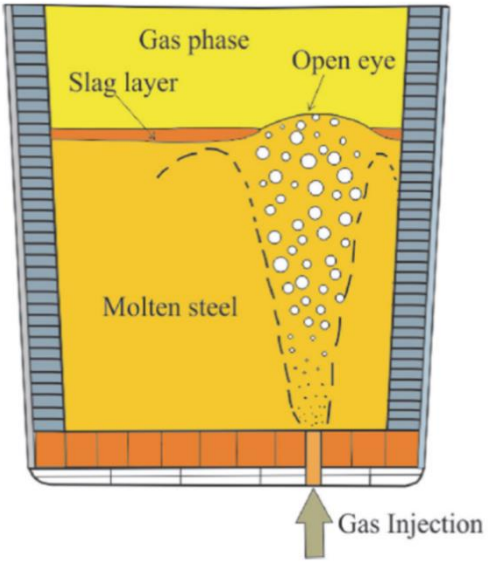

Fig.1 Schematic illustrating the ladle gas stirring process

Ladle purging is an essential process in steelmaking, specifically in secondary metallurgy, where the primary goal is to refine the molten steel to achieve the desired chemical composition and temperature before casting. The process involves injecting an inert gas (usually argon or nitrogen) through the bottom of the ladle to promote homogenization, remove non-metallic inclusions, and control the temperature. Here's a detailed explanation:

1.1 Purpose of Ladle Purging

I. Homogenization of the Molten Steel:
   - Temperature Uniformity: Ladle purging ensures that the temperature of the molten steel is uniform throughout the ladle. Since steelmaking involves handling large quantities of molten metal, temperature differences can exist between different layers. Purging helps in equalizing these temperature gradients.
   - Chemical Composition: Purging also aids in mixing the steel, ensuring that the alloying elements are evenly distributed, leading to a uniform chemical composition.

II. Removal of Non-Metallic Inclusions:
   - Floatation of Inclusions: Non-metallic inclusions, such as oxides, sulphides, and nitrides, can negatively affect the mechanical properties of the steel. Purging with an inert gas helps these inclusions float to the surface, where they can be removed as slag.
   - Inclusion Shape Control: The process also helps modify the shape of inclusions, which can be beneficial for improving the steel's ductility and toughness.

III. Desulfurization and Deoxidation:
   - Chemical Reactions: Purging can be used to promote chemical reactions that reduce the sulphur and oxygen content in the steel. For instance, injecting argon can help remove dissolved gases like hydrogen and oxygen, improving the steel's quality.

IV. Temperature Control:
   - Heat Transfer: Purging can also be used to control the heat transfer in the ladle. If the molten steel is too hot, purging can help dissipate some of the heat, whereas, in some cases, controlled purging can prevent excessive heat loss.

1.2 Ladle Purging Process

I. Ladle Design:
   - Porous Plugs: The ladle is equipped with porous plugs or tuyeres at the bottom through which the inert gas is injected. These plugs are designed to withstand the high temperatures and corrosive nature of the molten steel.
   - Gas Supply System: An argon or nitrogen supply system is connected to the ladle, allowing for precise control of gas flow.

II. Gas Injection:
   - Flow Rate: The flow rate of the inert gas is carefully controlled. A low flow rate is typically used to avoid excessive turbulence, which could lead to unwanted reoxidation or excessive slag entrapment in the steel.
   - Bubble Formation: The injected gas forms bubbles in the molten steel, which rise to the surface, promoting mixing and the removal of inclusions.

III. Monitoring and Control:

- Process Monitoring: The process is closely monitored to ensure that the desired effects are being achieved. Sensors may be used to measure the temperature, chemical composition, and other parameters.
- Automated Control: In modern steel plants, the purging process is often automated, with computer systems controlling the gas flow based on real-time data from the ladle.

IV. Post-Purging Operations:

- Slag Removal: After purging, the slag that has formed on the surface is removed. This slag contains the non-metallic inclusions and impurities that have been floated to the surface.
- Further Refinement: Depending on the steel grade and final requirements, additional treatments, such as alloying or vacuum degassing, may be performed after purging.

1.3 Advantages of Ladle Purging

- Improved Steel Quality: By promoting homogenization and removing inclusions, ladle purging improves the overall quality of the steel, leading to better mechanical properties.
- Efficiency: Ladle purging can reduce the time required for downstream processes, such as casting, by ensuring that the steel is in optimal condition.
- Cost-Effectiveness: By improving the efficiency of the steelmaking process and reducing defects, ladle purging contributes to cost savings in the production process.
- Improved homogeneity: Ladle purging helps to distribute alloying elements and temperature evenly throughout the molten metal. This uniformity in composition and temperature leads to better control over the final properties of the steel and prevents quality issues caused by inconsistencies.
- Reduced slag entrapment: By purging, the molten metal is kept in a more agitated state, which helps prevent slag from being entrapped in the metal, resulting in fewer inclusions and defects.

In summary, ladle purging is a critical process in steelmaking that enhances the quality and uniformity of molten steel by promoting homogenization, removing impurities, and controlling the temperature and chemical composition of the steel before casting.

1.4. Literature Review

1.4.1 Modelling of two-phase flows in gas-stirred ladles

The studies related to describing two-phase flow phenomena in a gas-stirred system are discussed in this section.

Szekely, Wang and Kiser [1] carried out experiments and numerical simulations for a water model of an argon-stirred ladle system. The simulation was performed by solving turbulent Navier-Stokes equations and were based on using Spalding's *k-ε* turbulent model. The results showed good agreement of flow velocity and gas fractions when compared to the experimental measurements. A similar kind of work was also done by Ilegbusi et al. [2] investigating the flow velocities in a water model of an argon gas-stirred ladle through experiments and simulations. The simulation results were compared for two different turbulent models (*k*- ε and anisotropic eddy viscosity model). The predicted simulation results of the mean velocity and turbulent parameters were compared to experimental measurements.

Xie and Oeters [3] and Xie, Orsten and Oeters [4] carried out experimental measurements to investigate the flow velocity in a ladle with liquid Wood's metal with nitrogen gas injected through centric blowing. The liquid flow field was measured using magnetic probes for various blowing conditions. Measurements were taken for the bubble behaviour, as well as the local gas fraction and the rising velocity of gas bubbles for different gas flow rates and nozzle diameters. The results were presented in the form of axial and radial velocities, the gas volume fraction and the turbulent kinetic energy at different heights of the ladle. The results showed that the flow is axially symmetric when gas was blown through a nozzle at a centric location. The flow velocity on the vessel axis was almost constant over the height and increased with an increasing gas flow rate and the nozzle diameter did not influence the flow velocity in the ladle.

Xia, Ahokainen and Holappa [5] carried out numerical simulations and validated the experimental measurements an axial and radial velocity profiles of Xie and Oeters [3], and Xie, Orsten and Oeters [4]. A Euler-Euler multi-phase model was used to describe the air and water phase in the ladle. Drag, lift and turbulent dispersion forces were used describe the momentum exchange between the two phases. The simulation results showed that the developed model provided an acceptable prediction of the fluid flow in the liquid region and a relatively large 22 deviation in the gas-liquid plume.

To describe two-phase flow phenomena in a gas stirred system for steel making Lou and Zhu [6] studied the influence of the turbulent dispersion force, as well as drag and lift forces on the liquid flow velocity, gas fraction and turbulent kinetic energy. The mathematical model developed was based on the Eulerian approach and the simulation results were compared to experimental results.

Mendez, Nigro and Cardona [7] performed a numerical simulation to study the effects of non-drag forces (virtual mass, lift and turbulent dispersion forces) on the gas fraction and liquid flow velocities in the ladle. A Eulerian modelling approach was used by Turkoglu and Farouk [8] to investigate the liquid flow velocity, gas fraction and

temperature fields in a cylindrical ladle through bottom air injection. The turbulence in the liquid phase was modelled using a two-equation *k-ε* turbulence model. The simulation results of the radial distribution of gas volume fraction and velocity measurements at specific axial locations were compared with experimental measurements available in the literature. The simulation results agreed well with the experimental results.

Davidson [9] conducted numerical simulations to investigate the magnitude of bubble rise velocity, centreline void fraction and the central plume in a liquid bath where gas was injected from the bottom. Domgin, Gardin and Brunet [10] carried out a detailed experimental and numerical study to investigate the mean velocity distribution and turbulent kinetic energy in a cylindrical steel bath where gas was injected through the bottom. The numerical simulations were performed based on Euler-Euler and Euler-Lagrange approaches. The simulations result of mean velocity profiles using the Euler-Euler approach were in good agreement compared to the Euler-Lagrangian approach when compared to with experimental results. A study of two different turbulence-modelling approaches (*k-ε* and RSM) was conducted by Park and Yang [11] for a gas stirred ladle system. The investigations included the flow velocities, gas fraction and turbulent kinetic energies. The results showed that the *k-ε* turbulence model was not suitable for predicting highly swirling flows, even though it yielded results that were in agreement with measurements in less swirling flows. The results also showed that the turbulent kinetic energies predicted by the *k*-ε model were higher than those predicted by the Reynolds stress model.

Recently Liu et al. [12] reviewed the research work carried out over a few decades into gas stirring in ladle metallurgy. This work presented the complete physical modelling and numerical simulations for four major areas: (1) mixing and homogenization in the ladle, (2) gas bubble formation, transformation, and 23 interactions in the plume zone; (3) inclusion behaviour at the steel-slag interface and molten steel; and (4) formation. They concluded that the mathematical models focusing on inclusion behaviour at the steel-slag interface needed to be improved.

1.4.2 Modelling of the fluid flow and open-eye formation in water model of a steel making ladle.

Studies related to open-eye formation in a water model ladle through physical modelling [13-22] and numerical simulations [25-33] have been performed extensively in the past three decades.

Yonezawa and Schwerdtfeger [13-15] carried out cold model measurements to investigate the open-eye size in a ladle using mercury and silicone oil to represent liquid metal and slag. The results concluded that the open-eye increased with an increase in the gas flow rate. A non-dimensional correlation was developed to represent the time-averaged open-eye size area. They also performed measurements to study the dynamics of spouts of gas plumes in a large-scale water model. In their work, a non-dimensional height, which is independent of the Froude number and nozzle diameter, was defined.

Based on the experimental data by Yonezawa and Schwerdtfeger [13-15], Krishnapisharody and Irons [16] proposed a model for estimating the plume eye area, which expresses the dimensionless eye area in terms of a density ratio of the fluids and Froude number shown in Equation (1).

$$A^* = \frac{A_e}{H^2} = \alpha + \beta \left(\frac{\rho}{\Delta\rho}\right)^{1\div 2} (Fr)^{1/2} \ldots\ldots\ldots\ldots\ldots\ldots (1)$$

where, α and β are numerical constants, $A*$ is the non-dimensional eye area, A is the open-eye area, H is height of the ladle, ρ is the density of water, $\Delta\rho$ is the density difference between water and oil, and Fr is the Froude number.

Krishnapisharody and Irons [17] further extended this model, developed a new one to predict the open-eye size from the primary operating variables of the ladle, and demonstrated its reliable predictive ability in a variety of multi-phase systems shown in Equation (2).

$$\frac{A_e^*}{A_p^*} = \alpha + \beta(1-\rho^*)^{-1\div 2}(Q^*)^{1\div 3}\left(\frac{H}{h}\right)^{1/2} \ldots\ldots\ldots\ldots (2)$$

The experimental studies that Krishnapisharody and Irons [16-17] performed in a cylindrical water model ladle concluded that the open-eye area increased with increasing the gas flow rates in all cases and decreased when the top phase thickness increased. An increase in the size of the open-eye with the increasing height of the water bath was also predicted from the results, although the enlargement is not linear. To study the effect of slag (oil) properties, three liquid-liquid systems were used: (1) a water-paraffin oil system; (2) an aqueous CaCl2 solution-paraffin oil system; (3) water-heavy motor oil. The results showed that the systems with less dense top phase systems had smaller s than denser top phase systems.

Wu, Valentin and Sichen [18] studied the open-eye formation in an argon stirred ladle using two physical models. To simulate liquid steel, water was used in both models. To simulate the slag, silicon oil was used in the first model and a Ga-In-Sn alloy was used

in the second model. The results showed that the open-eye size highly depends on the gas flow rate, the height of the lower liquid and the height of the top liquid. In contrast, the viscosity of the top liquid and interfacial tension between the two liquids has only a slight effect on the open-eye size. Similar work was carried out by Thuman et al. [19] where they used Ga–In–Sn alloy with a melting temperature of 283 K (10 °C) to simulate liquid steel and an MGCL2-glycerol (87%) solution to simulate the slag. It was found that no open-eye formed at lower flow rates, but that it did occur when the gas flow reached a critical rate. The critical flow rates were in the range of 0.7 to 4.0 NL/min and were found to depend greatly on the height of the top liquid.

Amaro-Villeda, Ramirez-Argaez and Conejo [20] studied the effect of the slag thickness on the open-eye area and the mixing time in the water model ladle. The slag thickness was varied in order to study its effect on the open-eye area and mixing time in a single plug system with a constant flow rate. A decrement of the open-eye area with an increase in slag thickness was observed. Maruyama and Iguchi [21] also performed cold model experiments in cylindrical vessel with a mercury-silicon oil system to study the effect of slag properties on the open-eye area. The results showed that the open-eye decreases with increases in the slag thickness and the density of the slag has effect on the open-eye size only when the thickness of slag exceeds a critical value. Mazumdar, Dhandpani and Saravanakumar [22] carried out experiments to measure the open-eye area in two different water models with a gas injection nozzle located at the mid bath radius position. Liu, Li and Li [23] performed measurements in a water model for studying the formation of the open-eye with different gas flow rates, slag layer thicknesses and number of nozzles. The results showed that the open-eye area increases approximately linearly as the gas flow rate increases. The open-eye area increases quickly with a reduction in the slag layer thickness showing that the slag layer thickness has a great influence on the open-eye area.

Several mathematical models have been developed to study the flow in the ladle. Li, Liu and Li [24] developed a mathematical model by using a multiphase volume of fluid (VOF) method coupled with a population balance model (PBM) to investigate the effect of the gas flow rate and plug radial position on the gas bubble diameter, and the open-eye size in the ladle. The open-eye size predicted by the numerical model agreed well with the experimental results and a critical gas flow rate to form a steady open-eye was found for the present water mode condition. Li et al. [25] developed a mathematical model based on large eddy simulations (LES) coupled with discrete particle modelling (DPM) and a VOF model to investigate the bubble movement and slag layer behaviour during the gas stirring process in the ladle. In this approach, a VOF model was used to track the liquid-slag-air interface and the Lagrangian DPM was used for describing the bubble movement. The simulation results showed that the bubbles were found to be moving in curved paths and that they induced many eddies in the region near the bubble plume. The shape and size of the open-eye was found to be irregular. At low flow rates, the open-eye formed and collapsed alternately and at high flow rates, the slag layer fluctuated and an open-eye was formed. The predicted simulation results of the formation and closing of the open-eye qualitatively agreed

with the experimental results from the water model. Li and Li [26] further extended the model developed by Li et al. [25] to investigate the bubble transport, bubble diameter redistribution, slag layer fluctuation and slag droplet generation in the water model ladle.

Calderon-Hurtadao et al. [27] performed both experiments and simulations to investigate the open-eye formation for different gas flow rates and slag layer thicknesses. For the experimental measurements, a velocity probe was placed close to the interface to monitor any turbulence. The results showed that the open-eye was found to be strongly dependent on the gas flow rate and slag layer thickness. Liu et al. [28] and Li, Li and Liu [29] investigated the effect of the gas flow rate and oil layer on the size, bubble movement and mixing time in a water model ladle through both physical and numerical modelling. The effect of the oil layer thickness was investigated by varying it from 20 to 40 mm and 50 mm for a constant flow rate in single-plug-stirred system. The results showed the oil thickness has a large influence on the open-eye area. The open-eye area increases quickly when the oil thickness decreases and vice-versa, although the increment is not linear.

Lv et al. [30] performed numerical simulations for a cold-water model, where water and sodium tungstate were employed to simulate liquid steel, and silicon oil was employed to simulate slag. The simulation results showed that the gas flow rate, bath height and slag layer thickness had strong effects on the open-eye size. Mazumdar and Guthrie [31-33], Mazumdar, Yadhav and Mahato [34], Mazumdar and Evans [35], Mandal, Madan and Mazumdhar [36], Peranadhanthan and Mazumdhar [37], Madan, Satish and Mazumdhar [38], Patil et al. [39], Subagyo, Brooks and Irons [40] and Guo, Gu and Irons [41] contributed to a greater extent towards investigating the fluid flow analysis and open-eye formation in the ladle. Furthermore, the work also extended to developing mathematical models to investigate the mixing time in ladles.

1.4.3 Modelling of the fluid flow and open-eye formation in an industrial scale ladle.

For industrial scale ladles, there are fewer experimental measurements for the open-eye formation available in the literature when the compared to water model ladle. This is due to the difficult conditions (e.g., high temperatures, process gases and dust) on the ladle surface, which make it quite hard to capture the process with a video camera.

Valentin et al. [42] captured the open-eye formation process in a 170-ton steelmaking ladle. The measurements included studying the effect of the stirring rate on the formation in the ladle. The trials were carried out by increasing the gas flow rate from 0 to 35 STP m3/h (583 SLM). At a flow rate of 15 STP m3/h (250 SLM), a circular shaped open-eye was generated approximately after two minutes of gas injection, shown in Figure 2. An increase of the flow rate to 25 STP m3/h (417 SLM) resulted in the formation of larger open-eyes and the change of the shape from circular to oval. A further increase of the flow rate to 35 STP m3/h (583 SLM) resulted in the formation of strong movements and turbulence on the surface and in the top slag as well as splashing and smoke formation. During the stirring process, circulating waves were detected on the surface at higher gas flow rates. Furthermore, numerical simulations were carried out to study the flow patterns for different gas flow rates.

Liu, Qi and Xu [43] numerically investigated a quasi-steady fluid flow and interfacial behaviour on the industrial scale ladle with argon gas injection through one plug, and two plugs placed in 1800 and 900 configurations, respectively. A VOF model was used to track the slag/steel/gas interface behaviour. The simulations were performed by increasing the flow rates from 50 to 400 L/min. The results showed that the bubble plume was not able to break the slag layer for a gas flow rate of 50 L/min. A small open-eye occurred when the flow rate was increased to 150 L/min and the open-eye size enlarged with an increase of the flow rate to 500 L/min. At high flow rates, the thickness of the slag layer became very thin near the sidewall of the ladle indicating a strong flow in the molten steel, which could damage the ladle wall refractory and reduce the ladle life. The results also concluded that the flow pattern of the molten steel was dependent on the plug configurations and gas flow rates. To avoid significant deformation of the slag layer, it was suggested to divide the gas flow into two weakened plumes by using a dual plug configuration. For a better refining process, the proper selection of the gas flow rate and plug configurations were proposed.

Li et al. [44] developed a mathematical model to analyse the transient three dimensional and three-phase flow in an argon stirred ladle with one and two off centred, porous plugs. Simulations were performed on a 220-ton industrial scale ladle, increasing the gas flow rates from 100 to 300 NL/min. The simulation results showed that the injected flow rate of argon gas had a significant effect on the spout peak height and the open-eye area. The diameter of the open-eye changed from 0.43 m to 0.81 m when the flow rate of argon gas varied from 100 to 300 NL/min. When argon gas was injected through two-plugs for a flow rate of 300 NL/min, two open-eyes were generated with diameters of about 0.6 m. As concluded by Liu, Qi and Xu [43], the

simulation results by Li et al. [44] also resulted in significant deformation of the slag layer during the stirring operation, and the slag thickness became thinner near the slag eye and thicker near the wall.

Singh et al. [45] developed a mathematical model to analyse a transient three phase flow in an industrial scale ladle with argon gas injecting from off-centred plugs. The VOF model, which was used by Liu, Qi and Xu [43] and Li et al. [44] was also used in this work to track the behaviour of the slag, steel and argon gas interfaces. At first, the simulation results of the open-eye area for different operating parameters were validated with the results by Liu, Qi and Xu [43]. The results showed that the open-eye area is very much dependent on the argon-stirring rate and slag layer thickness. Furthermore, the model predicted the desulfurization rate using chemical kinetic equations, as well as the interfacial area calculated from the CFD, and thermodynamic data obtained from the Thermo-Calc software. The results demonstrated that dual-plug configurations are more suitable for larger open-eye areas, which are needed for desulfurization, than the single plug configuration.

Gonzalez et al. [46] performed numerical simulations to study the flow pattern and open-eye formation in a steelmaking ladle under non-isothermal conditions. The results of thermal stratification and velocity fields were plotted on two vertical planes. The shape of the thermal stratification layers depends on the holding time owing to convective movement of steel according to the density difference. The flow field in the ladle reached a quasi-steady state condition after 20 seconds of argon gas injection.

Cloete, Eksteen and Bradshaw [47] also developed a full-scale, three-dimensional, transient mathematical model to study the fluid flow analysis in industrial scale ladles. The Lagrangian discrete phase model (DPM) was used to describe the bubble plume and the Eulerian VOF model for tracking the slag/steel/gas interface behaviour. The standard k □ ε model was used for modelling the turbulence. The results concluded that the model developed was computationally efficient for investigating the influence of a large number of operating and design variables on the fluid flow analysis and open-eye formation in the ladle. Cloete, Eksteen and Bradshaw [48] further extended this model to study the effect of plug arrangement on the flow analysis in the ladle.

Cao and Nastac [49] numerically investigated the fluid flow, mass transfer and slag-steel interface behaviour in a steelmaking ladle. In the first step, a Euler-Euler model was used to simulate the multi-phase flow in a water model and the results were validated with experimental results available from the literature. The Euler- Lagrange approach was used to study the effect of the free surface setup, injected bubble size, gas flow rate, and slag layer thickness on the slag-steel interaction and mass transfer behaviour. The argon gas floating process and open-eye formation process was investigated using both the VOF and DPM model. The gas rising upwards in the VOF model was continuous and concentrated and in the DPM model, the floating gas bubbles were dispersive and random. The decrement of the slag layer thickness resulted in the reduction in open-eye area and mass transfer coefficient in the molten

steel. When the gas flow rate was increased, the mass transfer coefficient and volumetric mass transfer coefficient in the molten steel became larger, and the open-eye area enlarged. Increase in the bubble size resulted in turbulence in the ladle becoming weaker and consequently the mass transfer coefficient in steel was reduced. Cao and Nastac [50] also modelled the transport and removal of inclusions in an industrial gas-stirred ladle. The effect of the gas flow rate, injected bubble diameters and the inclusion size on various removal mechanisms including slag capture, bubble attachment and ladle wall adhesion on the removal of inclusions was investigated.

1.4.4 Mixing and homogenization in the ladle

The studies related to describing the mixing phenomena in a water model and steelmaking ladle are discussed in this section.

Palovaara, Visuri and Fabritius [51] performed physical modelling measurements in a 1:5 scale water model of a 150-ton ladle to study the effect of the gas flow rate on the mixing phenomena. The mixing time was determined based on the change of the pH of the water bath using sulphuric acid as a tracer substance. The results indicated that the average mixing time decreases with increases in the gas flow rate non-linearly. Michaelek, Gryc and Moravka [52] studied the mixing phenomena through physical modelling in 1:10 scale water model. The mixing time was evaluated based on electrical conductivity and temperature changes, which were measured at three points in the ladle. The results obtained illustrated that the time required for homogenization decreased with an increase in the gas flow rate. Joo and Guthrie [53] investigated the mixing behaviour and mixing mechanisms as a function of the location of a porous plug, the tracer injection point, and ladle monitoring point. From the results, it was shown that eccentric bubbling gives steady results in terms of reducing the mixing times, since an angular momentum intermixes fluid across the width of the ladle.

Terrazas and Conejo [54] investigated mixing phenomena in a water model ladle. The measurements included studying the effect of process variables such as the nozzle diameter, gas flow rate and nozzle radial position on the mixing time. The mixing time decreased with an increase the nozzle diameter at low stirring rates, but at high stirring rates this effect was found to be relatively significant. The nozzle plug location played a pivotal role in the mixing time, and it is found that there was a large decrement in the mixing time when the radial position of the nozzle was changed from the centre of the ladle to a half radius position (i.e. to an eccentric position).

Conejo et al. [55] studied the effect of the top layer, nozzle arrangement, number of nozzles and gas flow rate on the mixing time in a 1:18 scale water model. The experimental results suggested that one nozzle located eccentrically at a distance of 0.67 R, with no slag, results in a shorter mixing time in comparison to two nozzles with separation angles of 180, 120, and 60 degrees, located at any radial distance. The mixing time decreased at low gas flow rates and increased at high gas flow rates, and in some cases, the slag layer thickness promoted a decrease in the mixing time.
Pan, Chaing and Hwang [56] investigated the effects of injection conditions on the mixing efficiency of the gas injection treatment in a water model. The results of these measurements concluded that the mixing efficiency was improved with increments of the gas flow rate and that an off-centre injection was better than centreline injection. Aoki et al. [57] investigated mixing phenomena in a bottom gas-stirred ladle through experiments and theoretical studies. Liu, Li and Li [23] studied the effect of gas flow rates and the number of porous plugs on the mixing time in a water model through physical modelling measurements.

Cao and Nastac [58] developed three-dimensional DPM-VOF coupled model to study the mixing phenomena in the industrial scale ladle. From the simulation results, it was found that two symmetrical plugs configuration provides higher mixing efficiency in the ladle when compared to one centric or one eccentric plug configuration. Lou and Zhu [59] developed a coupled model based computational fluid dynamics and population balance model (CFD-PBM) to investigate the effects of different numbers and positions of the nozzles, and the gas flow rate on the mixing phenomena in the 150-ton steelmaking ladle. The simulation results revealed that dual blowing gives a shorter mixing time in comparison to centric blowing configurations. The mixing time decreases with increase in the gas flow rate, and when the gas glow rate exceeds 300 NL/min the change in mixing time is small.

Geng, Lei and He [60] developed a mathematical model based on a two-phase fluid (Eulerian-Eulerian) to investigate the effect of the offset of dual plugs and the gas flow rate on the mixing time in a ladle with dual plugs. Ramirez-Argaez [61] performed calculations to study the effect of the gas flow rate, injector position, number of injectors, and ladle geometry on the mixing time. The simulation results showed that increments in the number of porous plugs resulted in longer mixing times. Haiyan et al. [62] numerically studied the effect of the gas flow rate, number, position and relative angle of porous plugs on the mixing time in the ladle. Zhu et al. [63] performed experiments and numerical simulations to study the mixing phenomena in an argon-stirred ladle with six types of porous plug arrangements. It was found that the porous plug arrangement has a significant effect on the mixing time.

Over the past decade, there have been relatively few studies on both physical and CFD modelling together with strong validation in studying the gas-steel-slag interface behaviour in the ladle. Moreover, the studies have focused more on modelling water models when compared to the modelling industrial ladles. In the current work, the simulation results of open-eye behaviour and mixing phenomena are provided with strong experimental data measured for validation and vice-versa. As for the experimental part, the work focuses on measuring the open-eye size for different flow rates, slag layer thickness and slag layer properties (density and viscosity) in water model and industrial measurements. The industrial measurements were performed at Outokumpu Stainless Oy in Tornio, Finland. As for the simulation part, the work focused on the development of the CFD model with the VOF approach to track the slag/steel/gas interface behaviour and species transport model for calculating the mixing time in the gas-stirred ladle.

1.5. Objectives of the work

The main objective of this thesis is to study the effect of different operating parameters i.e., argon gas purging rate, initial slag thickness, radial position(s) of the gas inlet(s) on the mixing time, wall shear stress and open eye formation process in a gas-stirred ladle.

The aims of this work are subdivided into three tasks shown below:

1. To formulate the mixing time, slag opening area and wall shear stress, dimensional analysis and empirical correlation has to use. because of their dependency on a number of parameters, including the angle of separation between the gas inlets, the radial position(s) of the gas inlet(s), the initial slag layer thickness and the argon gas purging rate.
2. To minimize the mixing time, slag opening area and wall shear stress, constrained multi-objective optimization with various optimization techniques i.e.genetic algorithm, particle swarm optimization, cuckoo-search optimization and teaching learning based optimization have to use to identify the optimal solution set.
3. To analyse the obtained optimal solution ANSYS software has to use for the validation.

2. Mathematical modelling

2.1Dimensional Analysis

The mixing time, slag opening area, and the maximum wall shear stress depend on several geometric and operating parameters like the radial and angular positions of the gas inlets, gas purging rate, slag layer thickness, and the metal bath height. A functional relationship was established between these variables, and Buckingham's P theorem was used to formulate a relationship between them in terms of dimensionless parameters as

$$\left[t_{mix}\sqrt{\frac{g}{H}}, \frac{A_s}{H^2}, \frac{\tau_{max}}{\rho_{st} g H}\right] = k_j \times \left(\frac{Q}{\sqrt{gH^5}}\right)^{a_j}$$

$$\left(\frac{h}{H}\right)^{b_j}\left(\frac{R_1}{H}\right)^{c_j}\left(\frac{R_2}{H}\right)^{d_j}\left(\frac{R_3}{H}\right)^{e_j}; j = 1-6 \ldots\ldots\ldots\ldots\ldots\ldots\ldots\ldots (3)$$

Here, to maintain dimensional consistency, the variable θ is replaced with the distance between the two gas inlets, which is defined as

$$R_3 = \sqrt{R_1^2 + R_2^2 - 2R_1R_2Cos\theta}$$

The eqn. (1) can be written in simplified form as

$$[t_{mix}, A_s, \tau_{max}] = k_j \times Q^{a_j} \times h^{b_j} \times R_1^{c_j} \times R_2^{d_j} \times R_3^{e_j}; j = 1-6 \ldots. (4)$$

Here, one must note that in the case of single purged ladle the second gas inlet does not exist and hence d_j and e_j becomes zero. A non-linear multiple regression analysis was done to determine the exponents a_j-e_j and the pre-exponent constant k_j.

2.2 Empirical Correlation

From the above analysis, it is clear that the mean shear stress depends on the design and operating parameters. A correlation was developed to predict the dimensionless wall shear stress for any configuration and operating conditions based on non-linear multiple regression analysis, as shown in Eqn. (3). To determine the constants *c*1, *a*, *b*, *c*, *d*, *e* in Eq. (4), as many as 40 numerical simulations were performed at various gas

flow rates, metal bath depth, slag thickness and inlet con-figurations. Based on the regression analysis, Eq. (4) can be rewritten as

$$\tau_{max} = 0.0014 \times Q^{0.516} \times h^{-0.228} \times R_1^{0.121} \ldots\ldots\ldots\ldots\ldots\ldots (5)$$

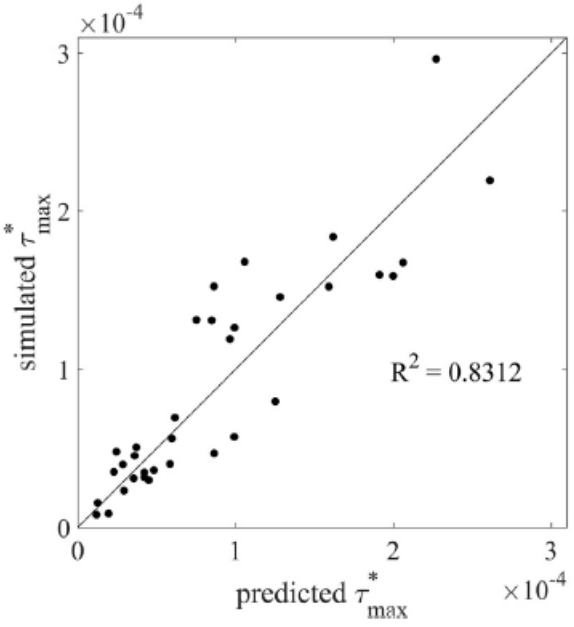

Regression Analysis fig. (2)

Eq. (5) provides the desired relationship between the wall shear stress and the design and operating variables, in dimensionless form. The maximum skin friction coefficient values that are predicted by the above equation, are shown in this Fig. 2, along with the maximum skin friction coefficient values that were obtained from numerical simulations. It is clear from this figure that Eq. (5) is adequate to characterize wall shear stresses in dual plug fitted industrial scale steel making ladles, at various operating conditions, with in the range of values considered in the present study.

Fig. (3) shows the variation of maximum skin friction coefficient with dimensionless values of gas flow rate, metal bath depth, slag thickness and configuration of gas inlets. The maximum skin friction coefficient increases by increasing the dimensionless gas flow rate, dimensionless radial distance of injectors from the base centre or by decreasing the dimensionless distance between both the inlets and dimensionless slag thickness. From these figures, as well as from Eq. (5), it is clear that the dimensionless skin friction coefficient is largely dependent on the dimensionless gas purging rate and on the dimensionless radial distance of injectors from the centre of the gas inlets.

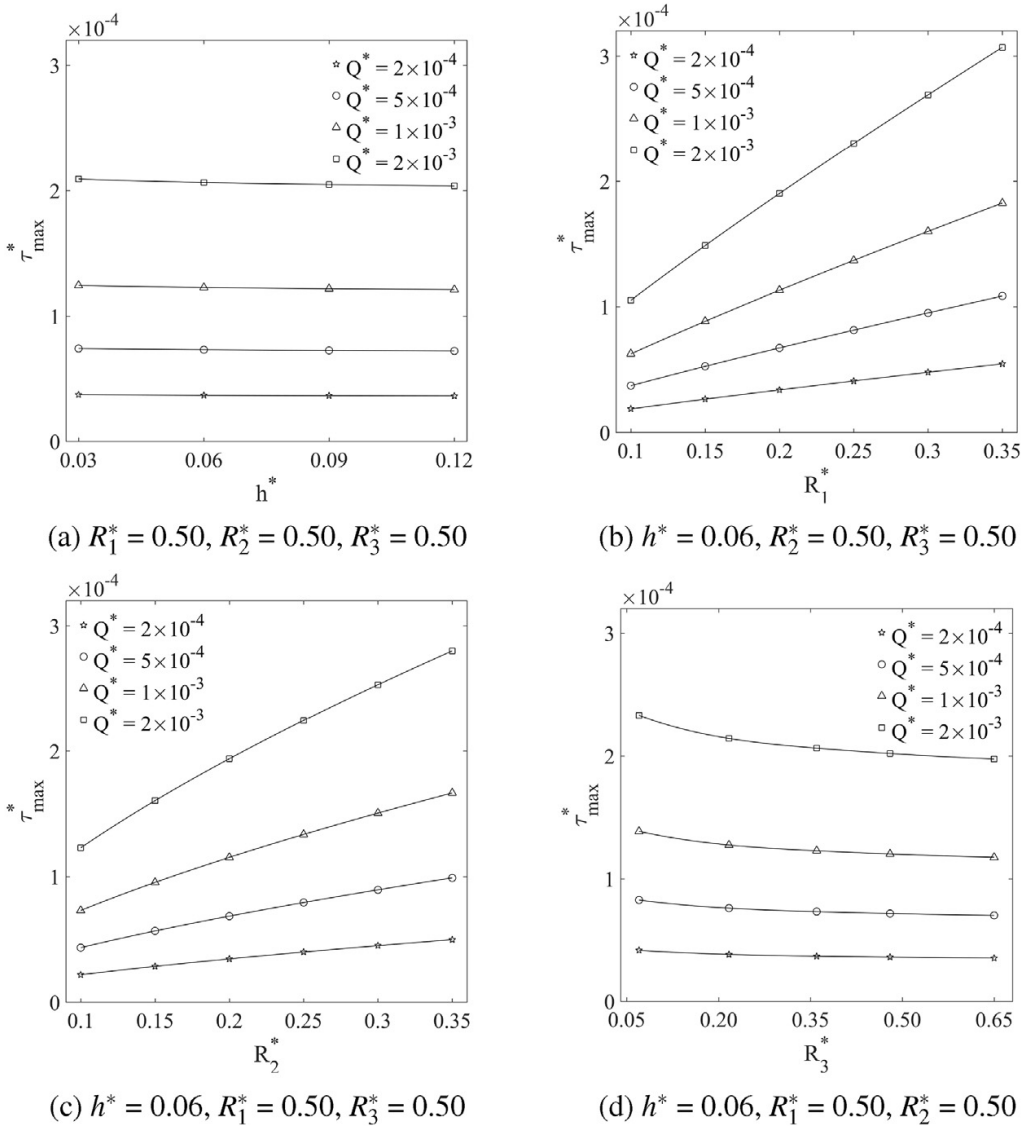

(a) $R_1^* = 0.50$, $R_2^* = 0.50$, $R_3^* = 0.50$

(b) $h^* = 0.06$, $R_2^* = 0.50$, $R_3^* = 0.50$

(c) $h^* = 0.06$, $R_1^* = 0.50$, $R_3^* = 0.50$

(d) $h^* = 0.06$, $R_1^* = 0.50$, $R_2^* = 0.50$

Fig. (3) Variation of maximum skin friction coefficient

Variation of maximum skin friction coefficient with non-dimensional design and operating parameters.

Similarly, based on non-linear multiple regression analysis the exponents a_j-e_j and the preexponent constant e_j in eqn. (4) were determined. Accordingly, the empirical correlations for estimating the value of mixing time, slag opening area, and maximum wall shear stress respectively in single purged industrial ladles are obtained as

2.2.1 Objective Functions for single purged ladle

$$t_{mix} = 15.48 \times Q^{-0.319} \times h^{0.086} \times R_1^{-0.037} \ldots\ldots\ldots\ldots\ldots (6)$$

$$A_s = 2.991 \times Q^{0.745} \times h^{-0.882} \times R_1^{0.036} \ldots\ldots\ldots\ldots\ldots\ldots\ldots (7)$$

$$\tau_{max} = 0.0014 \times Q^{0.516} \times h^{-0.228} \times R_1^{0.121} \ldots\ldots\ldots\ldots\ldots\ldots (8)$$

Subjected to,

$$2.02 \text{ X } 10^{-4} \leq \text{Q}^* \leq 20.20 \text{ X } 10^{-4}$$

$$0.025 \leq \text{h}^* \leq 0.10$$

$$3.25 \text{ X } 10^{-4} \leq \text{R1}^* \leq 0.325$$

$$9.60\ X\ 10^{-2} \leq R2^* \leq 0.325$$

2.2.2 Objective Functions for Dual Purged Ladle

$$t_{mix} = 15.96 \times Q^{-0.324} \times h^{0.055} \times R_1^{-0.061} \times R_2^{-0.069} \times R_3^{0.113} \ldots\ldots (9)$$

$$A_S = 0.566 \times Q^{-0.685} \times h^{-1.061} \times R_1^{0.079} \times R_2^{0.057} \times R_3^{-0.207} \ldots\ldots\ldots\ldots (10)$$

$$\tau_{max} = 0.1883 \times Q^{0.7494} \times h^{-0.0194} \times R_1^{0.8548} \times R_2^{0.6572} \times R_3^{-0.0742} \ldots\ldots\ldots\ldots\ldots\ldots\ldots (11)$$

Subjected to,

$$2.02 \text{ X } 10^{-4} \leq \text{Q}^* \leq 20.20 \text{ X } 10^{-4}$$

$$0.025 \leq \text{h}^* \leq 0.10$$

$$3.25 \text{ X } 10^{-4} \leq \text{R1}^* \leq 0.325$$

$$9.60\ X\ 10^{-2} \leq R2^* \leq 0.325$$

$$9.56\ X\ 10^{-2} \leq R3^* \leq 0.650$$

The coefficient of determination R2 of the regression obtained for all the above correlations ranges between 0.80 and 0.94. it can be seen from eqn. 6-11 that in the mixing time increases with an increase in the slag layer thickness or with a decrease in the gas purging rate and the radial distance of the gas inlet. In dual purged ladles, the mixing time increases with the angle between the two gas inlets. Similarly, the slag opening area and the maximum wall shear stress increases with an increase in the inlet

gas purging rate and the radial distance of the gas inlet from the centre and decreases with an increase in initial slag layer thickness. During dual bottom purging the slag opening area and the maximum wall shear stress also decreases with an angle between the gas inlets.

Equations 6–8 and Equations. 9–11 is considered the objective functions for the optimization problem in single purged and dual purged ladles, respectively.
From the exponents of the variables in these equations, one can observe that the objective functions have opposing natures. Therefore, a unique optimal solution does not exist. Instead, a collection of many solutions is produced, and at each point, the objective functions are optimum. Such a set of solutions is called a Pareto optimal solution set. Pareto optimal solutions are those where an improvement in one objective function can only be achieved with a deterioration of at least one of the other objective functions. In the objective space, all the Pareto optimal solution points together form a Pareto front. With the constraints to the decision variables, the Pareto optimal solution set is obtained by solving the multi-objective optimization problem.

3. Optimization

3.1 Optimization by genetic algorithm

A Genetic Algorithm (GA) is a search heuristic that is inspired by Charles Darwin's theory of natural evolution. It reflects the process of natural selection where the fittest individuals are selected for reproduction to produce offspring of the next generation. Genetic algorithms are widely used for optimization and search problems where traditional methods may not be as effective.

3.1.1 Steps and Concepts in Genetic Algorithms

I. Population**:**
- A set of potential solutions to the problem at hand. Each individual in the population represents a possible solution.
- These individuals are typically represented by chromosomes, which can be strings of binary, real numbers, or other formats depending on the problem.

II. Chromosome**:**
- A chromosome is a single solution to the problem, often represented as a string (binary, real numbers, or other forms).
- Each chromosome consists of genes, which are individual elements of the string, representing specific characteristics of the solution.

III. Gene**:**
- A gene is a part of the chromosome, representing a specific trait or decision variable in the solution.

IV. Fitness Function:
- The fitness function evaluates how good or bad a solution (chromosome) is. It assigns a fitness score to each individual in the population.
- The goal is to maximize or minimize the fitness function depending on the problem.

V. Selection**:**
- The selection process chooses the fittest individuals from the population to be parents and pass their genes to the next generation.
- Common selection methods include roulette wheel selection, tournament selection, and rank-based selection.

VI. Crossover (Recombination)**:**
- Crossover is a genetic operator used to combine the genetic information of two parent chromosomes to produce new offspring.
- There are several types of cross-over, such as single-point crossover, two-point crossover, and uniform crossover.

VII. Mutation**:**

- Mutation introduces diversity into the population by randomly altering the genes of a chromosome.
- It helps to prevent the algorithm from becoming stuck in local optima by exploring new regions of the solution space.

VIII. Termination:

- The algorithm continues to evolve the population through selection, crossover, and mutation until a termination condition is met.
- Common termination conditions include reaching a maximum number of generations, achieving a satisfactory fitness level, or convergence of the population.

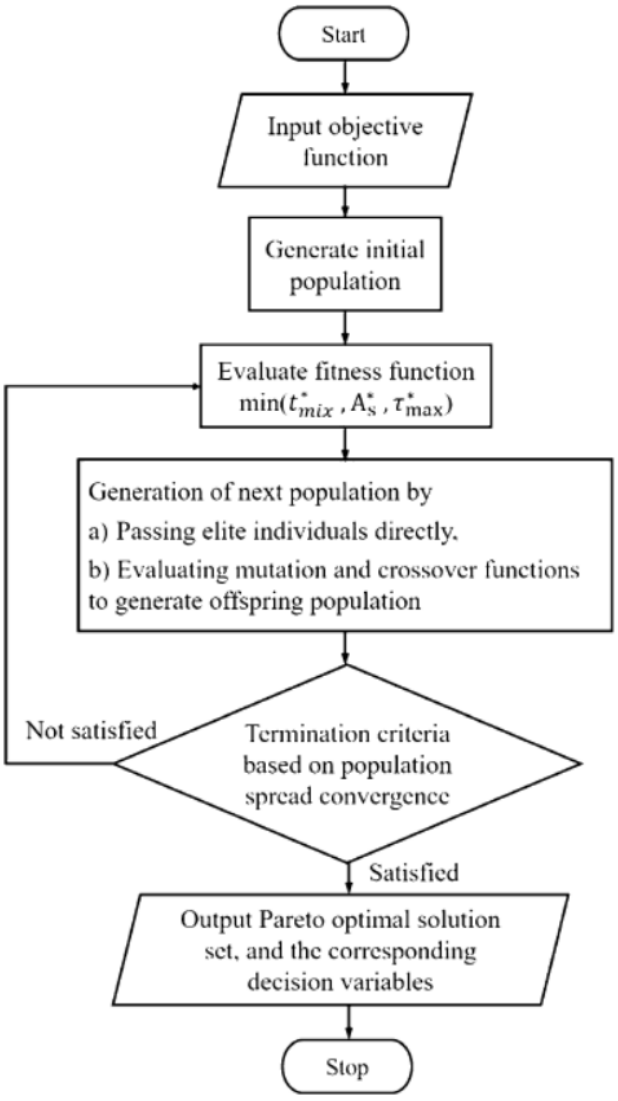

Fig.4 Flow chart of GA

3.1.2 Advantages

- Versatility: GAs can be applied to a wide range of optimization problems.
- Global Search Capability: Genetic algorithms are less likely to get stuck in local optima compared to traditional optimization methods.
- Parallelism: GAs can be easily parallelized, making them efficient for large-scale problems.

Genetic Algorithms are powerful tools for solving complex optimization problems, particularly when the solution space is large, and traditional methods are not feasible. They mimic the process of natural evolution, making them flexible and adaptable to a wide range of applications.

Genetic Algorithms are powerful tools for solving complex optimization problems, particularly when the solution space is large, and traditional methods are not feasible. They mimic the process of natural evolution, making them flexible and adaptable to a wide range of applications.

3.2 Optimization by particle swarm algorithm

Particle Swarm Optimization (PSO) is a computational method used for solving optimization problems, inspired by the social behaviour of birds flocking or fish schooling. It was developed by James Kennedy and Russell Eberhart in 1995. PSO is a population-based stochastic optimization technique, meaning it uses a population of candidate solutions (particles) that move around in the search space to find the optimal solution.

3.2.1 Steps and Concepts in Particle Swarm Optimization

I. Particles**:**
- Each particle represents a potential solution to the optimization problem.
- Particles are characterized by their position (which represents a candidate solution) and velocity (which determines how the particle moves through the search space).

II. Swarm**:**
- The entire group of particles is called the swarm.
- The swarm collectively moves through the solution space, searching for the optimal solution.

III. Fitness Function**:**
- The fitness function evaluates how good a particular solution (particle's position) is. It assigns a fitness value to each particle.
- The goal is to maximize or minimize the fitness function depending on the problem.

IV. Velocity Update**:**
- The velocity of each particle is updated based on three components:
- Inertia: This represents the particle's tendency to continue moving in the same direction as before.
- Cognitive Component (Self-knowledge)**:** This component drives the particle towards its best-known position (personal best, p_{best}).
- Social Component (Swarm Influence)**:** This component drives the particle towards the best-known position in the entire swarm (global best, g_{best}).
- The velocity update equation is typically given by:

$$v_i(t+1) = \omega . v_i(t) + c_1 . r_1 . \left(p_{best,i} - x_i(t)\right) + c_2 . r_2 . \left(g_{best} - x_i(t)\right)$$

$v_i(t)$ is current velocity of particle *i.*

ω is the inertia weight

c_1 and c_2 are cognitive and social coefficient respectively.

r_1 and r_2 are random numbers uniformly distributed in the range [0,1]

$x_i(t)$ is the current position of particle *i*.

V. Position Update:

- After updating the velocity, the particle's position is updated by:

$$x_i(t+1) = x_i(t) + v_i(t+1)$$

This new position represents the particle's new potential solution.

VI. Personal Best

- Each particle keeps track of its own best position (i.e., the position that has given the best fitness value so far).

VII. Global Best

- The swarm also keeps track of the best position encountered by any particle in the swarm (i.e., the best fitness value found by any particle).

VIII. Swarm Convergence:

- Over time, particles tend to converge towards the best solutions found by the swarm, which ideally leads to finding the optimal solution.

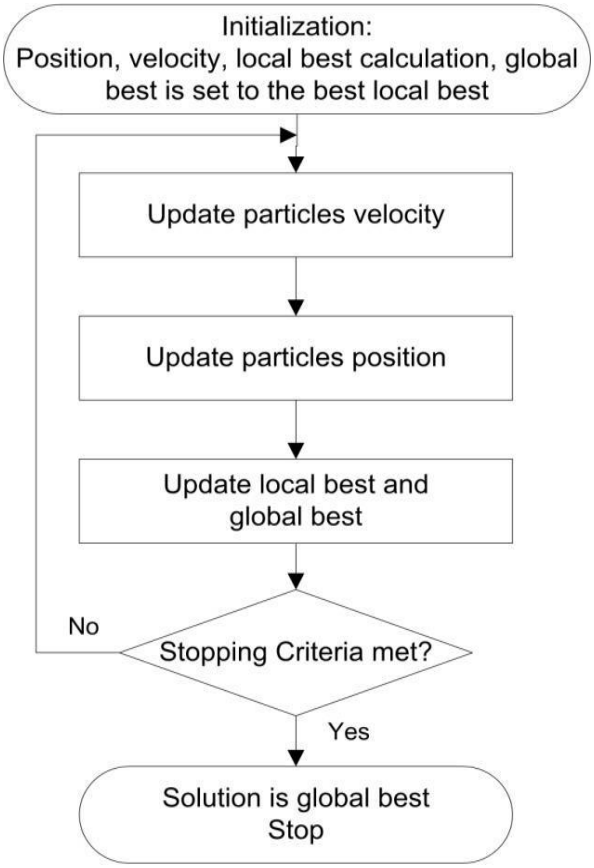

Fig.5 Flow chart of PSO

3.2.2 Advantages

- Simplicity: PSO is easy to implement and requires few parameters to adjust.
- Efficiency: It is computationally less expensive compared to other evolutionary algorithms like Genetic Algorithms (GAs).
- Parallelism: Like GAs, PSO can be easily parallelized, making it suitable for large-scale problems.
- No Derivatives Needed: PSO does not require the gradient of the fitness function, making it suitable for non-differentiable, noisy, or complex objective functions.

Particle Swarm Optimization is a robust and versatile optimization technique, making it suitable for a wide range of applications, particularly when the problem landscape is complex or poorly understood.

3.3 Optimization by teaching learning - based algorithm

Teaching-Learning-Based Optimization (TLBO) is a population-based optimization algorithm inspired by the teaching and learning process in a classroom. It was introduced by R. V. Rao, V. J. Savsani, and D. P. Vakharia in 2011. TLBO mimics the influence of a teacher on learners and the interactions among learners to improve their knowledge, which is analogous to finding an optimal solution in the search space.

3.3.1 Steps and Concepts in TLBO

I. Population (Classroom)**:**

- The population in TLBO is analogous to a classroom of students (learners), where each learner represents a candidate solution to the optimization problem.
- The quality of each learner's solution is analogous to the learner's knowledge or performance, evaluated using a fitness function.

II. Teacher**:**

- The teacher is the best solution in the current population (the learner with the highest fitness).
- The role of the teacher is to enhance the knowledge level of the learners by moving them towards the teacher's level.

III. Learners**:**

- Learners are the individuals in the population, each representing a potential solution to the problem.
- Learners interact with the teacher and with other learners to improve their knowledge (i.e., improve their solutions).

IV. Fitness Function**:**

- The fitness function evaluates how good or bad a particular solution is. It assigns a fitness value to each learner (solution).
- The goal is to maximize or minimize the fitness function depending on the problem.

❖ Phases in TLBO

- TLBO operates in two main phases: the **Teacher Phase** and the **Learner Phase**.

I. Teacher Phase**:**

- In this phase, the teacher (best solution) tries to improve the knowledge of the learners.
- The teacher influences the learners by moving them closer to the teacher's knowledge level. This is done by adjusting the learners' positions in the search space based on the difference between the mean knowledge level of the class and the teacher's knowledge level.
- The position update for a learner *i* is given by:

$$\boldsymbol{X_{i,new} = X_i + r.\left(X_{teacher} - T_f.X_{mean}\right)}$$

Where;

$\boldsymbol{X_{i,new}}$ is the updated position of learner *i*.

$\boldsymbol{X_i}$ is the current position of learner i.

$\boldsymbol{X_{teacher}}$ is the position of teacher.

$\boldsymbol{X_{mean}}$ is the mean position of all learners**.**

$\boldsymbol{T_f}$ is the teaching factor, usually set to either 1or 2 representing the

Level of influence the teacher can have.

r is a random number in the range [0,1]

- After updating the learners' positions, their fitness values are evaluated, and the best solution (teacher) is updated if necessary.

II. Learner Phase**:**

- In the learner phase, learners interact with each other to enhance their knowledge.
- A learner i interacts with another randomly selected learner j. If learner j has a better fitness, learner i moves closer to j's position. Otherwise, learner i moves away from j's position to explore a different region of the search space.
- The position update for a learner iii after interaction with learner j is given by:

If $f\left(X_j\right) < f(X_i)$

$$X_{i,new} = X_i + r\,.\left(X_j - X_i\right)$$

If $f\left(X_j\right) \geq f(X_I)$

$$X_{i,new} = X_i + r\,.\left(X_i - X_j\right)$$

Where;

$X_{i,new}$ is the updated position of learner i.
X_i and X_j are the current positions of learners I and j respectively.
$f(X_i)$ and $f(X_j)$ are the fitness value of learner I and j, respectively.
r is the random number in the range [0,1].

After the interaction, the new positions are evaluated and the best solution (teacher) is updated if necessary.

III. Termination**:**

- The TLBO process is repeated, cycling through the Teacher and Learner phases until a termination condition is met. Common termination conditions include reaching a maximum number of iterations, achieving a satisfactory fitness level, or observing convergence in the population.

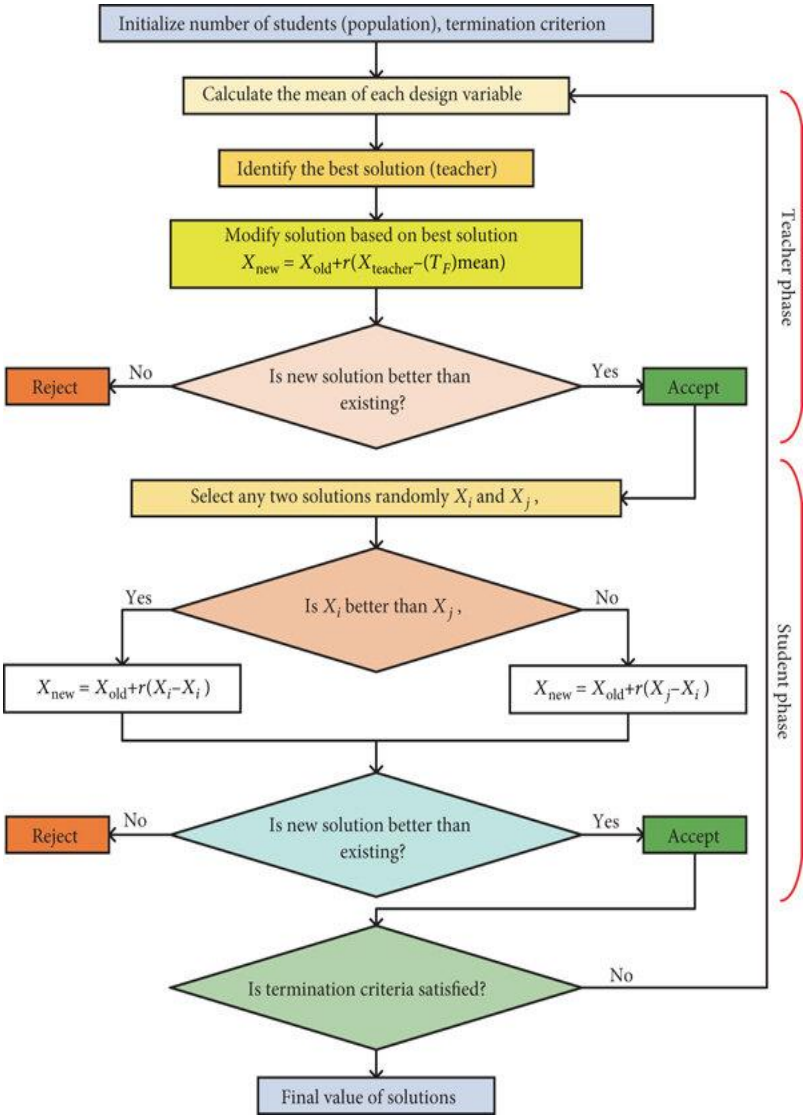

Fig.6 Flow chart of TLBO

3.3.2 Advantages

- Simple and Easy to Implement: TLBO does not require tuning of algorithm-specific parameters (like crossover rate, mutation rate, etc.), making it easy to implement and apply.
- No Algorithm-Specific Parameters: TLBO is free from algorithm-specific parameters, which simplifies the tuning process and makes it easier to apply across different problems.
- Effective for Various Optimization Problems: TLBO has been successfully applied to a wide range of optimization problems, including constrained, unconstrained, and multi-objective problems.
- Efficient: TLBO generally converges quickly, making it computationally efficient.

Teaching-Learning-Based Optimization is a powerful and versatile optimization technique that mimics the educational process. Its simplicity, lack of algorithm-specific parameters, and effectiveness in solving a wide range of optimization problems make it an attractive choice for researchers and practitioners alike.

3.4 Optimization by cuckoo search algorithm

Cuckoo Search (CS) is a nature-inspired optimization algorithm developed by Xin-She Yang and Suash Deb in 2009. It is based on the brood parasitism of some cuckoo species, particularly their habit of laying eggs in the nests of other birds. The CS algorithm also incorporates the Lévy flight behaviour of birds and fruit flies, which is a type of random walk where the step lengths have a probability distribution that is heavy-tailed.

3.4.1 Steps and Concepts in Cuckoo Search

I. Cuckoo Behaviour**:**
- Some species of cuckoos lay their eggs in the nests of other host birds (of different species). If the host bird discovers the egg is not its own, it may either throw the egg away or abandon the nest and build a new one elsewhere.
- Cuckoo Search simulates this parasitic behaviour where each cuckoo represents a solution, and its egg represents a new candidate solution. The goal is to replace worse solutions (host bird's eggs) with better ones (cuckoo's eggs).

II. Lévy Flights**:**
- Lévy flight is a random walk where the steps are drawn from a Lévy distribution, which is a heavy-tailed probability distribution. This means that the cuckoos can make large jumps, allowing for a more extensive exploration of the search space.
- In the context of optimization, Lévy flights help the algorithm escape local optima and explore new regions of the solution space.

III. Fitness Function**:**
- The fitness function evaluates how good a solution is, assigning a fitness value to each cuckoo (solution).
- The goal is to maximize or minimize the fitness function, depending on the problem.

IV. Host Nests**:**
- The population of potential solutions in CS is referred to as nests. Each nest contains an egg representing a solution to the optimization problem.
- The quality of the nests is evaluated based on the fitness function.

V. Termination**:**
- The process of generating new solutions via Lévy flights, evaluating fitness, replacing nests, and abandoning poor nests continues until a termination condition is met.
- Common termination conditions include reaching a maximum number of iterations, achieving a satisfactory fitness level, or observing convergence in the population.

❖ Steps in cuckoo search

I. initialization
- A population of nests (solutions) is initialized with random positions in the search space.
- Each nest contains an egg, which represents a candidate solution.

II. Cuckoo generation (via levy flights);
- A new solution (cuckoo egg) is generated by performing a Lévy flight from the current solution.
- The position update for a solution is given by;

$$x_{new} = x_{old} + \alpha . Levy(\lambda)$$

Where;
α is the step size scaling factor.
$Levy(\lambda)$ represents a step drawn from a levy distribution with exponent λ
- Lévy flights result in occasional large steps, allowing for global exploration of the search space.

III. Fitness evaluation and replacement
- The fitness of the newly generated cuckoo (new solution) is compared to the fitness of a randomly chosen nest.
- If the new solution is better (has a higher fitness), it replaces the existing solution in the nest.

IV. Host nest abandonment
- A fraction p_α of the worst nests is abandoned, and new nests are built randomly in different locations (random solutions are generated).
- This step introduces diversity into the population and helps the algorithm escape local optima.

V. Termination
- The process of generating new solutions via Lévy flights, evaluating fitness, replacing nests, and abandoning poor nests continues until a termination condition is met.
- Common termination conditions include reaching a maximum number of iterations, achieving a satisfactory fitness level, or observing convergence in the population.

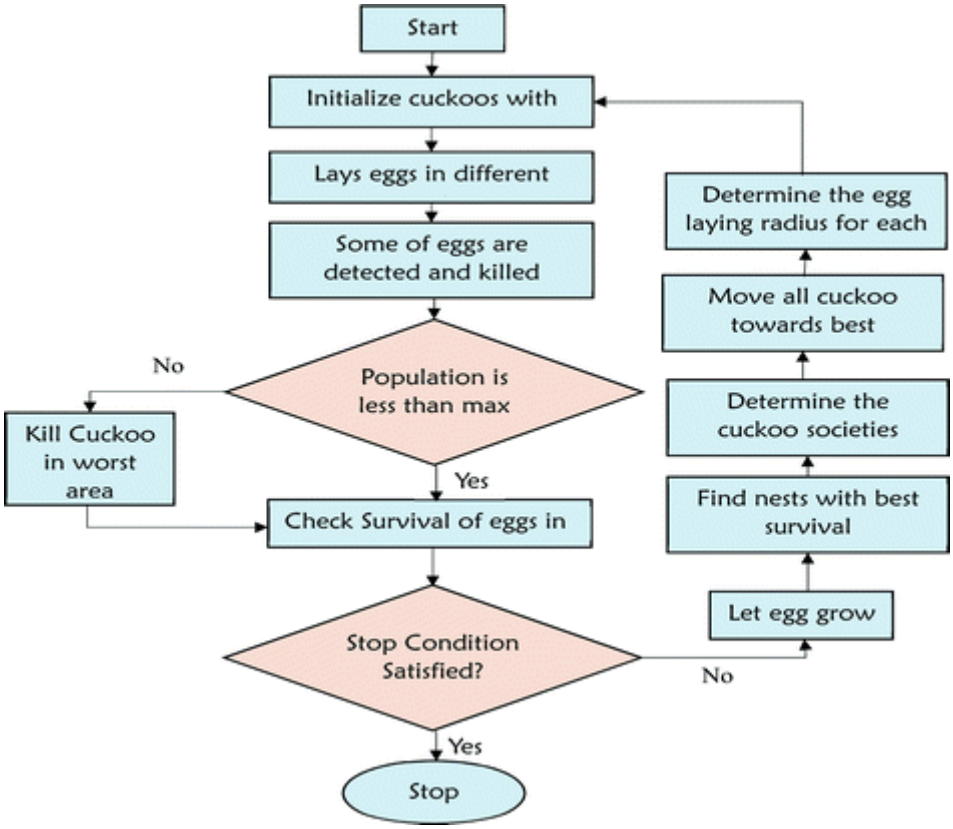

Fig.7 Flow chart of CSO

3.4.2 Advantages

- Global Search Capability: The use of Lévy flights allows Cuckoo Search to perform a global search and avoid getting stuck in local optima, making it effective for complex optimization problems.
- Simple and Easy to Implement: CS has few parameters to adjust, making it simple and easy to implement.
- Efficient Exploration and Exploitation: The balance between exploration (global search) and exploitation (local search) is effectively managed by the Lévy flight mechanism and the host nest replacement strategy.
- Good Performance on Multimodal Functions: CS is particularly effective in handling multimodal functions, where the search space has multiple peaks and valleys.

Cuckoo Search is a powerful and versatile optimization technique, particularly suited for solving complex, multimodal optimization problems. Its simplicity, efficiency, and ability to avoid local optima make it a valuable tool for a wide range of applications.

4. Analysis using Ansys software

4.1 Description of the analysis

In the current work, a VOF model was used to solve the three-phase flow and to track the slag/steel/gas interface behaviour in the ladle. The following governing equations of the VOF model and turbulence model need to be solved.

4.1.1 Conservation equations

The continuity and momentum equations are shown in Equations (3) and (4), respectively.

Continuity equation

$$\frac{\partial \rho}{\partial t} + \frac{\partial (\rho x_i)}{\partial x_i} = 0 \quad \text{..... (12)}$$

. Momentum equation

$$\frac{\partial (\rho u_i)}{\partial t} + \frac{\partial (u_i\, u_j)}{\partial x_j} = -\frac{\partial \rho}{\partial x_i} + \frac{\partial}{\partial x_j}\left[\mu_{eff.}\left(\frac{\partial u_i}{\partial x_j} + \frac{\partial u_j}{\partial x_i}\right)\right] + F_i + F_{vol},$$

..... (13)

where F_i is the body force in the case of gas blowing in the ladle and F_{vol} is the volume force which the source term for surface tension, given by

$$F_i = \alpha \rho_l g_i \quad \text{..... (14)}$$

$$F_{vol} = \sigma_{ij}\, \frac{\rho k_i \nabla \alpha_i}{1 \div 2\,(\rho_i + \rho_j)} \quad \text{..... (15)}$$

4.2.2 Turbulence models

The standard k-ε equation is used to model the turbulence, which solves two equations for the transport of turbulent kinetic energy and its dissipation rate to obtain the effective viscosity field.

$$\rho \frac{\partial k}{\partial t} + \frac{\partial(\rho k u_i)}{\partial x_i} = \frac{\partial}{\partial x_i}\left[\left(\mu + \frac{\mu_t}{\sigma_k}\right)\frac{\partial k}{\partial x_i}\right] + G_k - \rho\varepsilon \quad \ldots\ldots\ldots\ldots (16)$$

$$\rho \frac{\partial \varepsilon}{\partial t} + \frac{\partial(\rho \varepsilon u_i)}{\partial x_i} = \frac{\partial}{\partial x_i}\left[\left(\mu + \frac{\mu_t}{\sigma_\varepsilon}\right)\frac{\partial \varepsilon}{\partial x_i}\right] + C_{1\varepsilon}\frac{\varepsilon}{k}\left(G_k + C_{3\varepsilon}G_b\right) - C_{2\varepsilon}\rho\left(\frac{\varepsilon^2}{k}\right) \ldots\ldots (17)$$

where k is the turbulent kinetic energy, ε is the turbulent dissipation rate, and x_i represents the spatial coordinates for different directions. G_k is the turbulent kinetic energy source term caused by mean velocity gradients, and G_b is the turbulent kinetic energy source term caused by buoyancy. These terms are calculated by Equations (9) and (10).

$$G_k = -\rho u_i u_j \frac{\partial u_i}{\partial u_j} \quad \ldots\ldots\ldots\ldots\ldots (18)$$

$$G_b = -g_i\left(\frac{\mu_t}{\rho} Pr_t\right)\frac{\partial \rho}{\partial x_i} \quad \ldots\ldots\ldots\ldots (19)$$

$$\mu_t = \frac{\rho C_u k^2}{\varepsilon} \quad \ldots\ldots\ldots\ldots\ldots\ldots (20)$$

The turbulent viscosity is calculated by Equation (20) using k and ε from Equations (16) and (17) respectively. The constants k and ε used in the present study were recommended by Launder and Spalding [79].

4.2.3 The volume of fluid model

The Volume of Fluid (VOF) model can be used to track the interface between the phases by solving a single set of momentum equation. In this work, the tracking of the interfaces between liquid steel/slag/top-gas is accomplished using this model. The governing equation can be written as follows:

$$\frac{1}{\rho_k}\left[\frac{\partial}{\partial t}\left(\alpha_q\rho_q\right) + \nabla .\ \alpha_q\rho_q v_q\right] = S_{\alpha_q} + \sum_{\rho=1}^{n}(\dot{m}p_q - \dot{m}q_p) \ldots\ldots\ldots \text{(21)}$$

where $\dot{m}pq$, $\dot{m}qp$ represent the mass transfer from phase p to q and phase q to p in unit time and volume, respectively; α_q is the volume fraction of phase q, ρ_q is the density of phase q, S_{α_q} is the source term taken as 0 in the Fluent software. The volume fraction of the main phase is not calculated in the Fluent software, while it can be acquired by Equation (22). When the volume fractions are summing the following equation is satisfied:

$$\sum_{q=1}^{n}\alpha_q = 1 \ldots\ldots\ldots\ldots\ldots \text{(22)}$$

4.2.4 Species transport model

To calculate the mixing process in the ladle, the species transport model was solved throughout the computational domain

$$\frac{\partial(\rho c)}{\partial t} + \nabla.(\rho u c) = \nabla.\left[\rho\left(D + \frac{\mu_t}{\rho Sc_t}\right)\nabla c\right] \ldots\ldots\ldots\ldots\ldots\ldots (23)$$

where *D* is the mass diffusion coefficient and Sc_t is the turbulent Schmidt number with a default value of 0.7 ($Sc_t = \frac{\mu_t}{\rho D_t}$ = where D_t is the turbulent diffusivity).

4.3 Geometry Meshing and Boundary conditions

4.3.1 Industrial scale model

A160 tonne capacity, industrial scale ladle has been considered for the present study. The geometry details and the properties of all the constituent phases are obtained from the literature (Liu et al., 2011; Llanos et al.,2010). Multiple gas inlets were considered at various radial and angular positions. The schematic representation of the computational domain and the gas inlet configuration on the base of the ladle are shown in Fig. (5). A com-bination of any two of the inlets was used for purging of argon gas into the metal bath, for a single case.

Initially, the ladle was filled with molten steel, with a floating slag layer on the top which was open to the atmosphere.

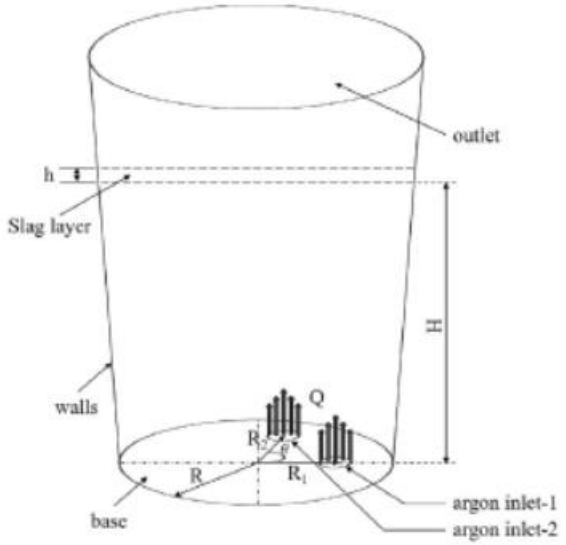

Fig.8 Geometry

Table 1: Fluid properties

Property	Value
Steel density	7020 kg/m^3
Steel viscosity	0.006 kg/m-s
Slag density	3500 kg/m^3
Slag viscosity	0.2664 kg/m-s
Argon density	1.6228 kg/m^3
Argon viscosity	0.000021 kg/m-s
Surf. Tension slag/steel	0.12 N/m
Surf. Tension steel/argon	1.192 N/m
Air density	1.225 kg/m^3

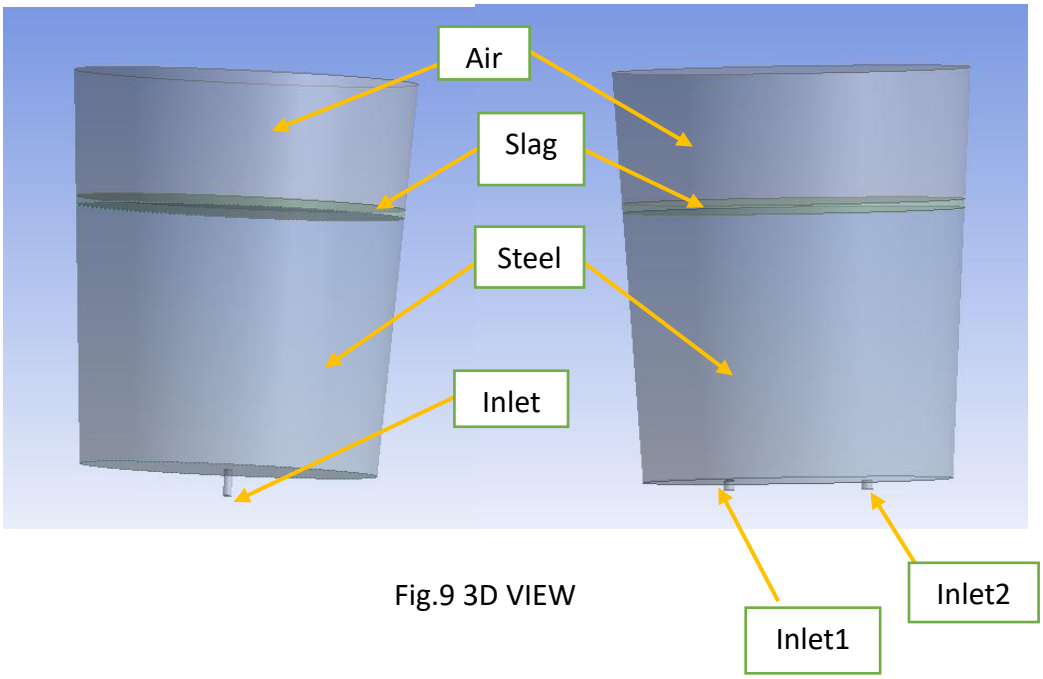

Fig.9 3D VIEW

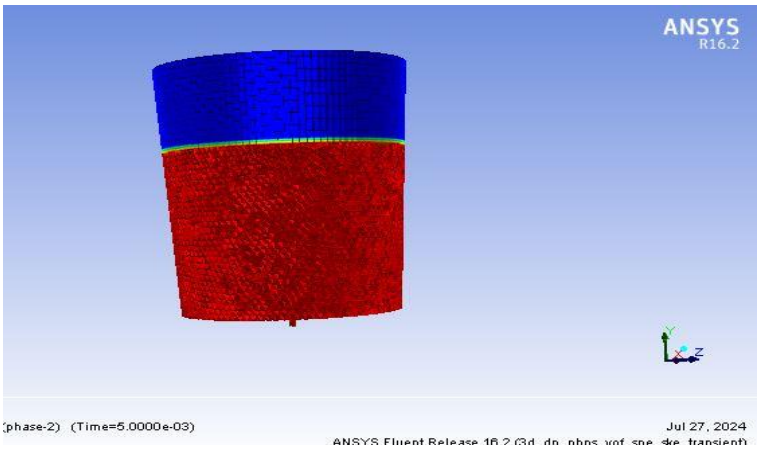

Fig.10 Volume fraction distribution

Boundary conditions

S.No	Boundary name	Boundary condition
1	Inlet	ρ_{ar} α_{ar} v_{in} = constant; $k = \frac{3}{2}(v_{avg}\ I)^2$; $\omega = 0.09^{-\frac{1}{4}}\frac{\sqrt{k}}{l}$
2	Base	$\vec{v} = 0, k = 0, \omega = 0$
3	Walls	$\vec{v} = 0, k = 0, \omega = 0$
4	Outlet	P = 101325 Pa, $k = \frac{3}{2}(v_{avg}\ I)^2$, $\omega = 0.09^{-\frac{1}{4}}\ \frac{\sqrt{k}}{l}$

Fig.11

The computational domain and mesh

Figure 11 displays the boundary conditions and computational mesh for the industrial scale ladle setups. Hexahedral elements were created in a structured mesh using the ANSYS ICEM CFD program. By establishing the maximum mesh size of 8 mm for the entire domain and 4 mm for the inlet and slag layer, a mesh with roughly 1 million cells was produced. With an explicit geo-construct scheme, the interface was tracked during the simulations using the volume of fluid (VOF) model in the ANSYS Fluent program. For the industrial size ladle, the same boundary conditions as in the water model covered in section 3.3.1 above were applied.

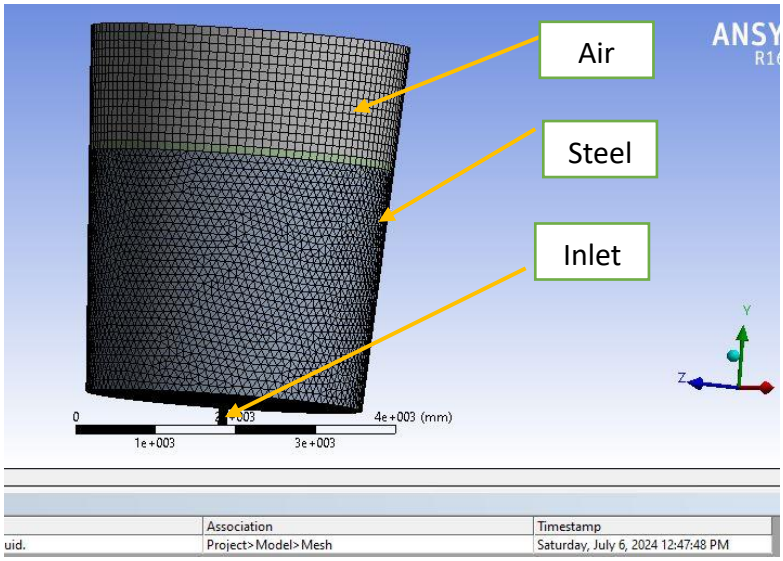

Fig. 12 Mesh geometry of single purged ladle

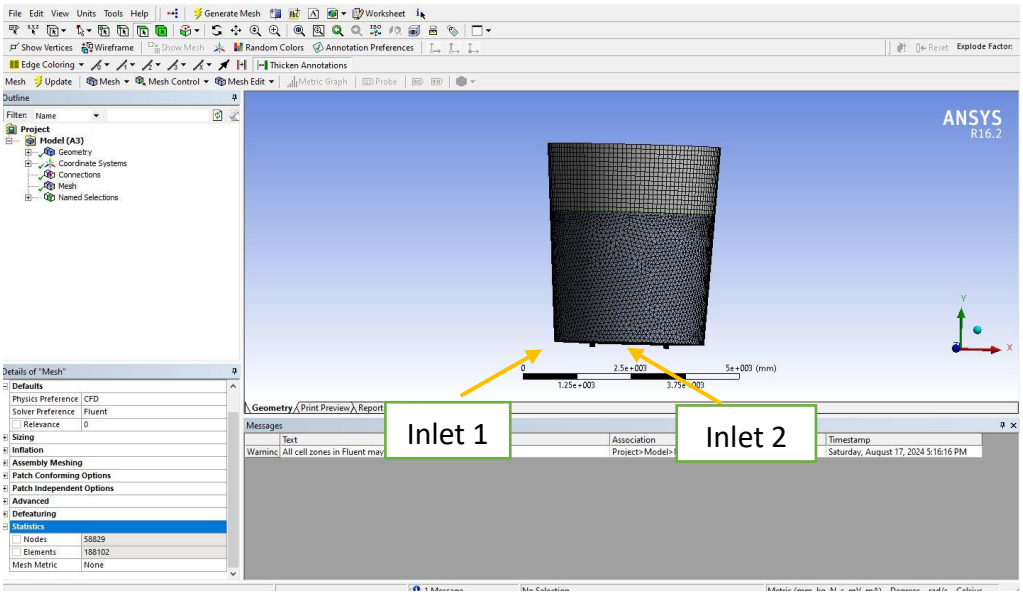

Fig.13 Mesh geometry of dual purged ladle

5. Optimum Results

5.1 Genetic Algorithm

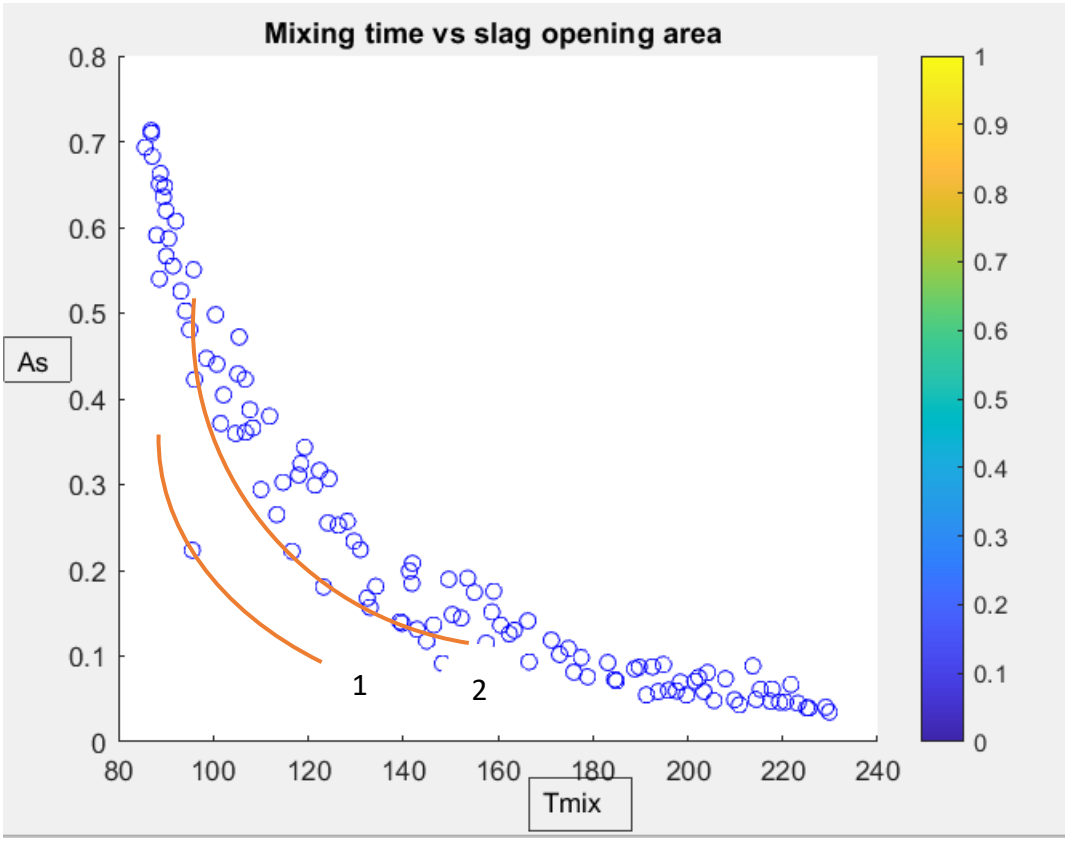

Fig.14 Mixing time vs slag opening area

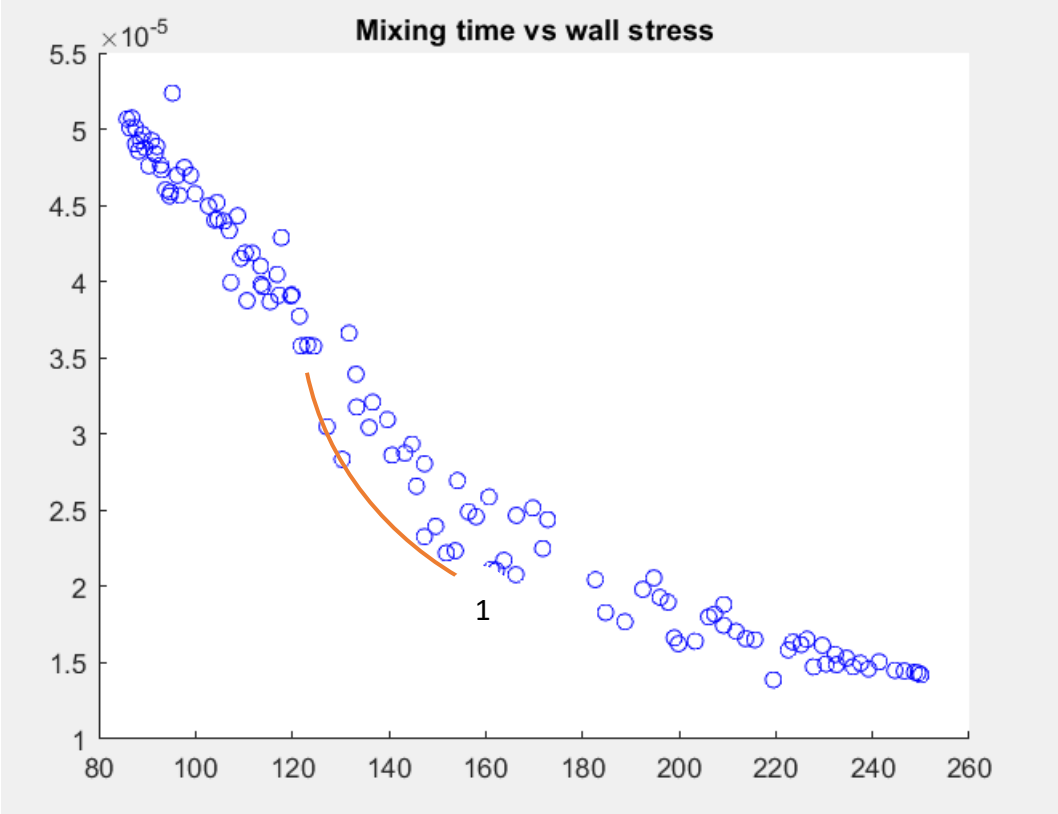

Fig.15 Mixing time vs wall shear stress

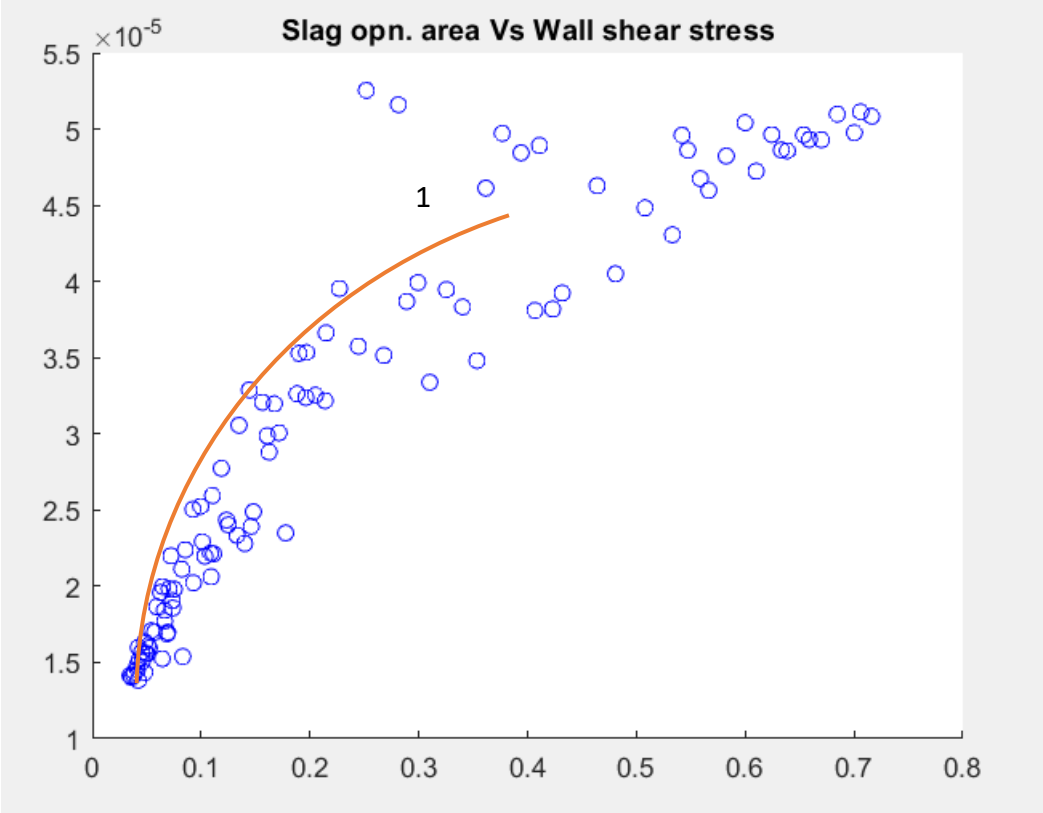

Fig. 16 Slag opening Area vs wall shear stress

TABLE 2: Some Optimal Results

t_{mix}	τ_{max}	Q	h	$R1$
229.0737	0.00001	0.0002	0.0888	0.0012
217.7713	0.00002	0.0002	0.0538	0.0026
225.5558	0.00001	0.0002	0.0936	0.0021
85.6456	0.00004	0.0020	0.0264	0.3193
88.6302	0.00001	0.0020	0.0272	0.1548
162.3860	0.00004	0.0005	0.0502	0.0036
184.9356	0.00003	0.0003	0.0651	0.0216
197.5981	0.00002	0.0003	0.0711	0.0106
202.3084	0.00001	0.0003	0.0508	0.0034
213.7006	0.00005	0.0002	0.0339	0.0022
94.1502	0.00006	0.0020	0.0351	0.0503
223.2137	0.00001	0.0002	0.0768	0.0034
96.0846	0.00001	0.0019	0.0419	0.0560

5.2 Cuckoo-search optimization

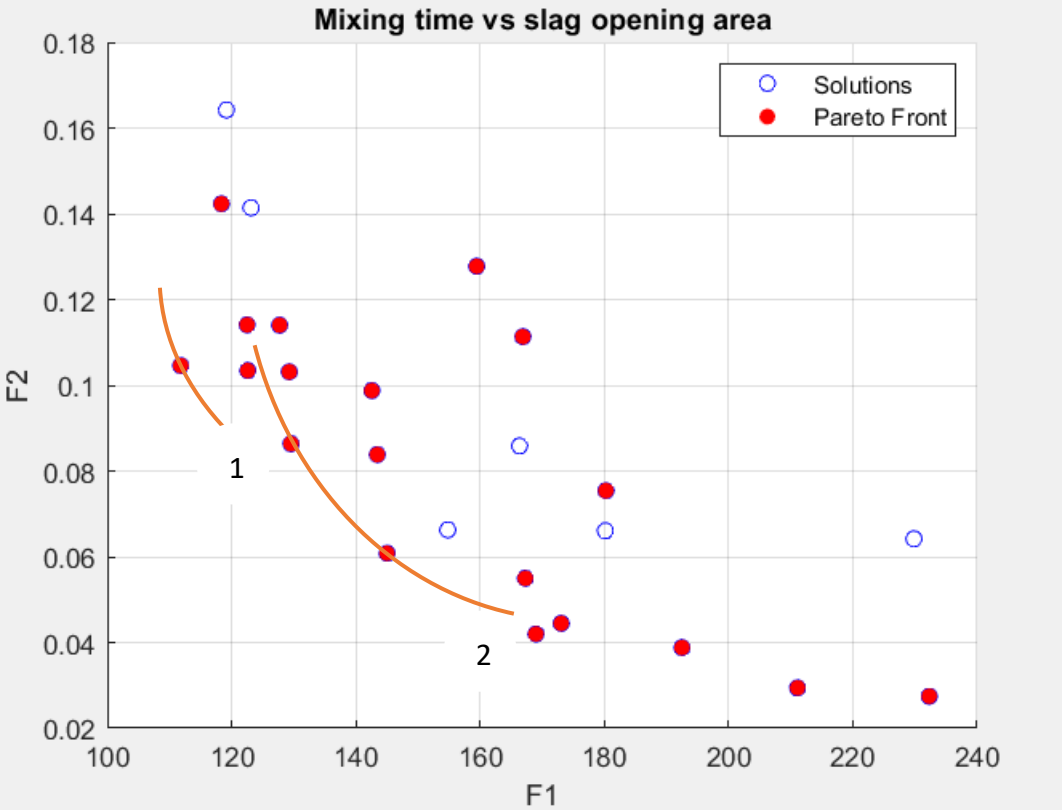

Fig. 17 Mixing time vs slag opening area

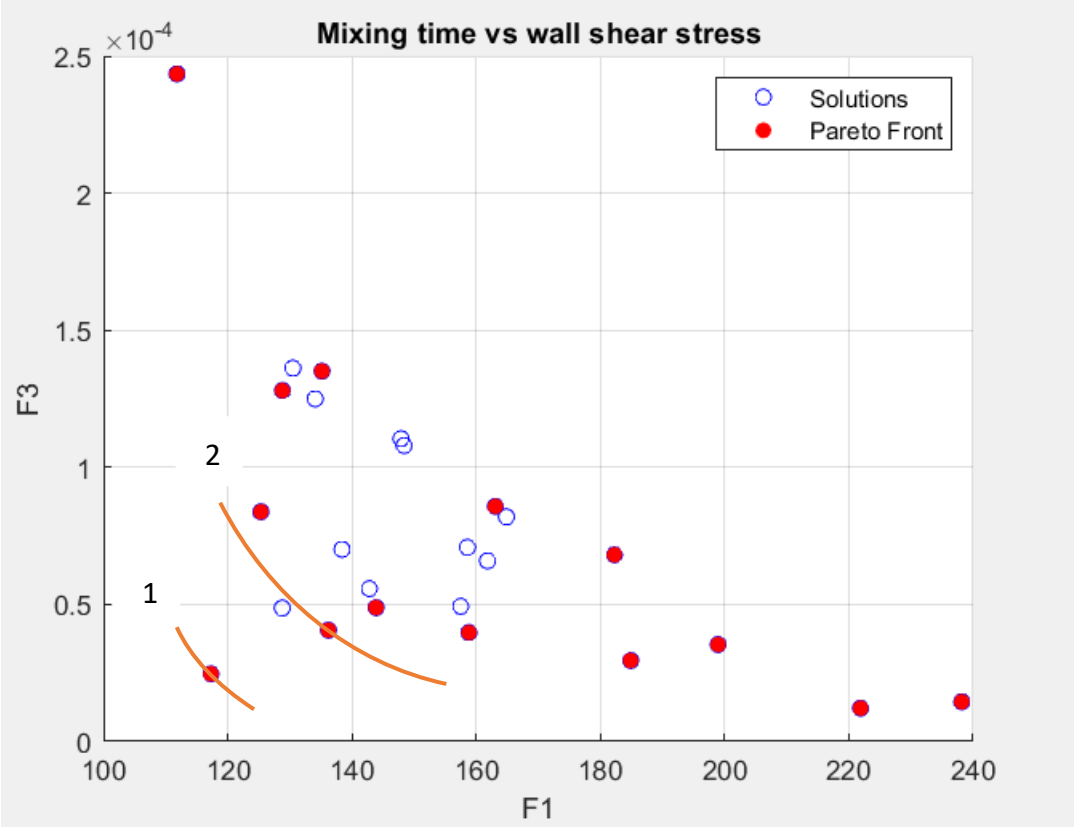

Fig. 18 Mixing time vs wall shear stress

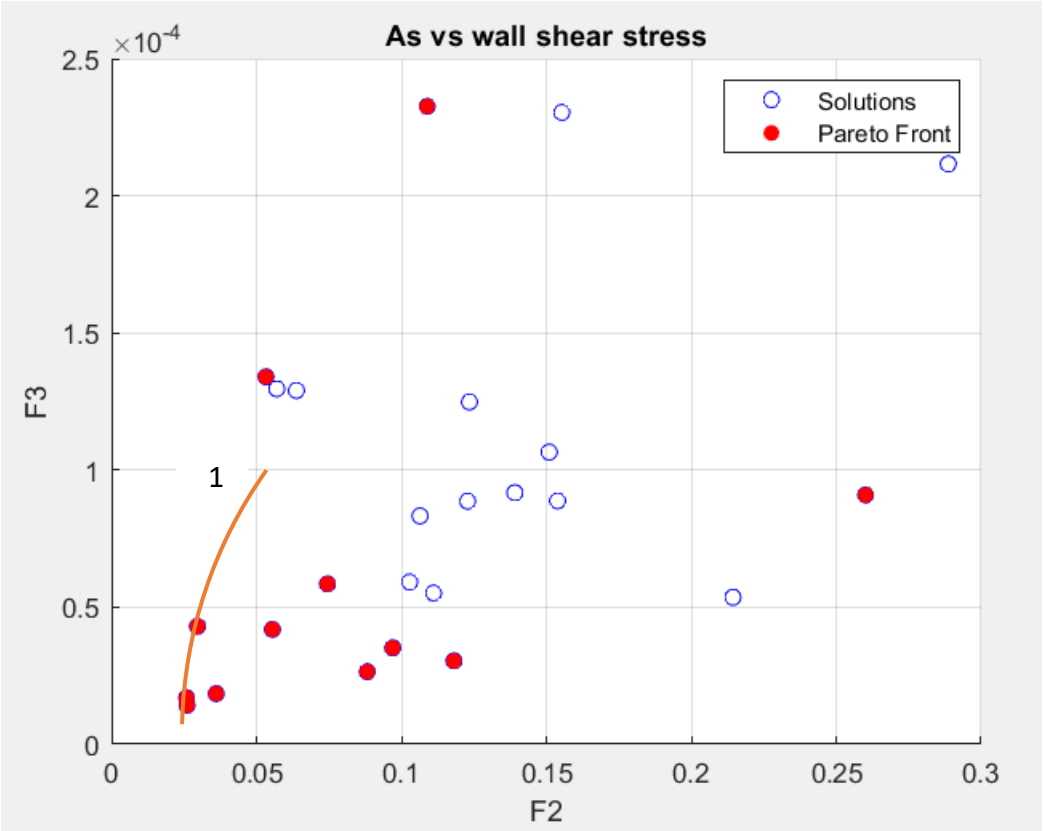

Fig.19 slag opening area vs wall shear stress

5.3 Teaching-learning based optimization

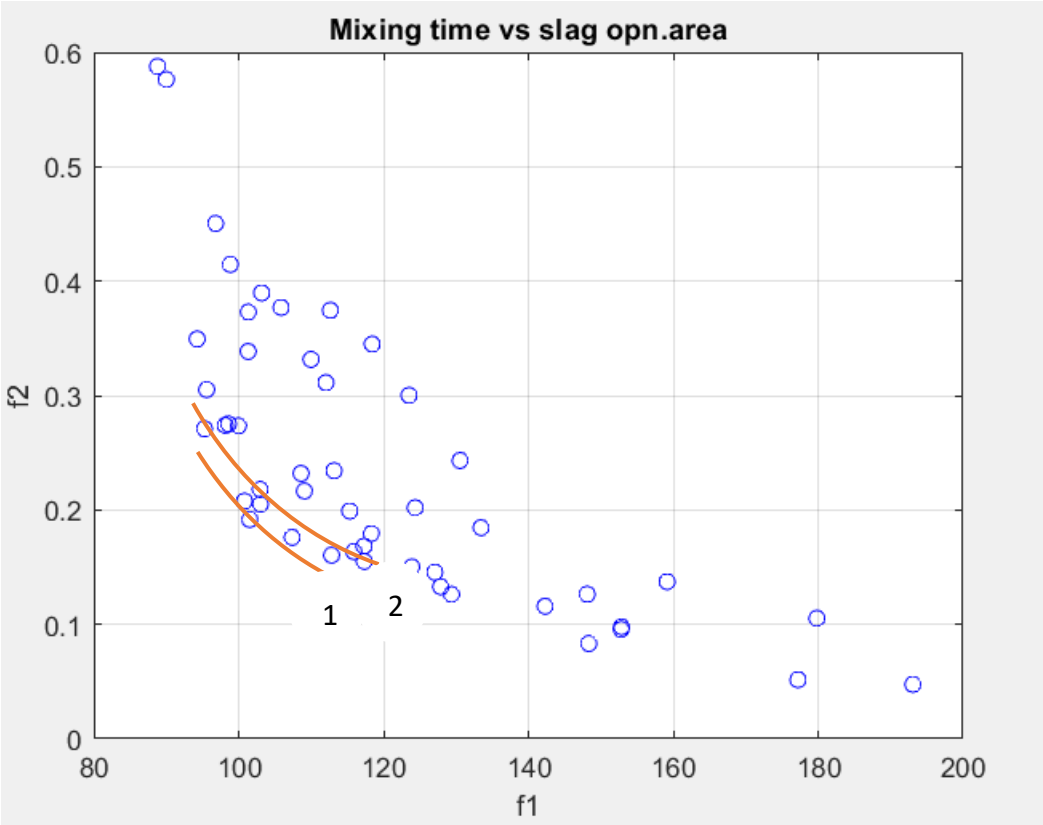

Fig.20 Mixing time vs slag opening area

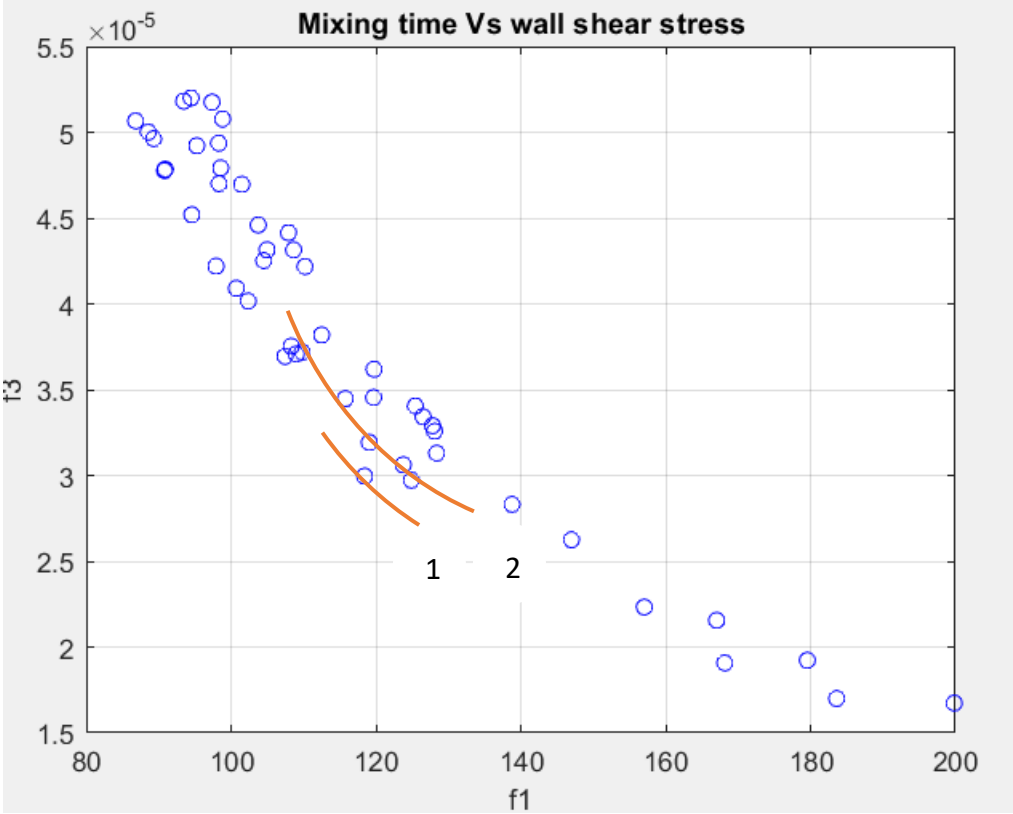

Fig.21

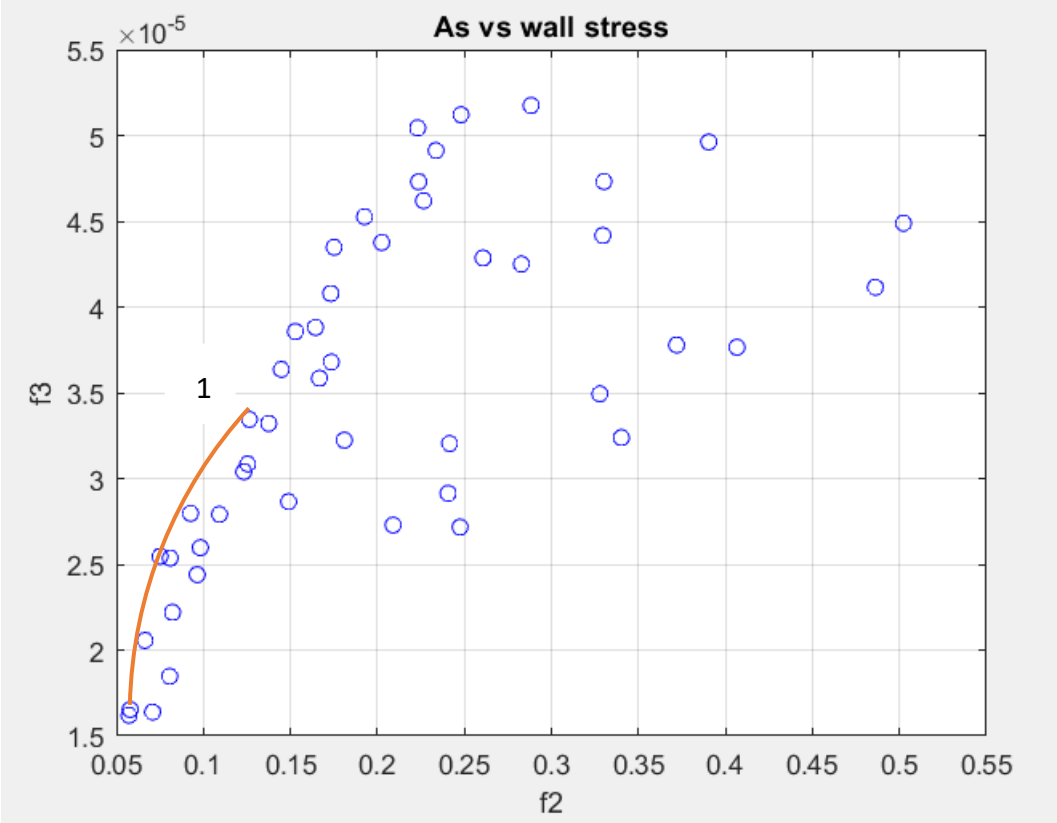

Fig.22 slag opening area vs wall shear stress

5.4 Particle Swarm Optimization

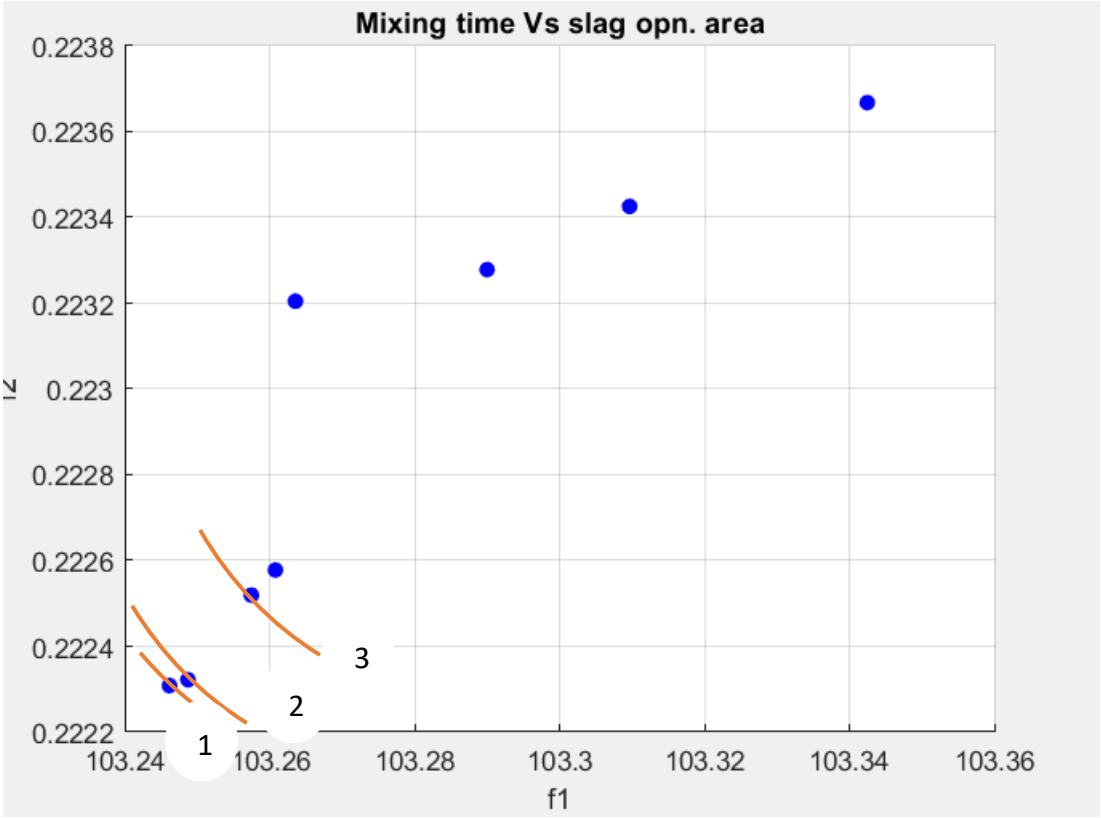

Fig.23 Mixing time vs slag opening area

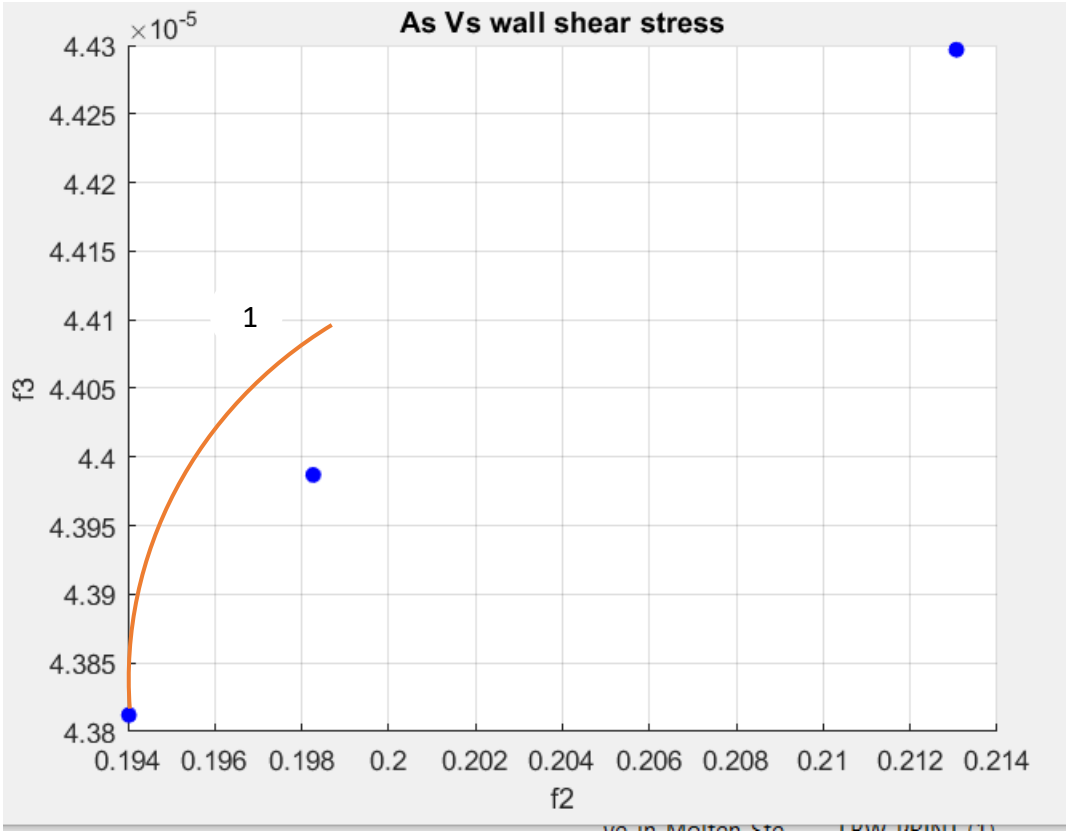

Fig.24 Slag opening area vs wall shear stress

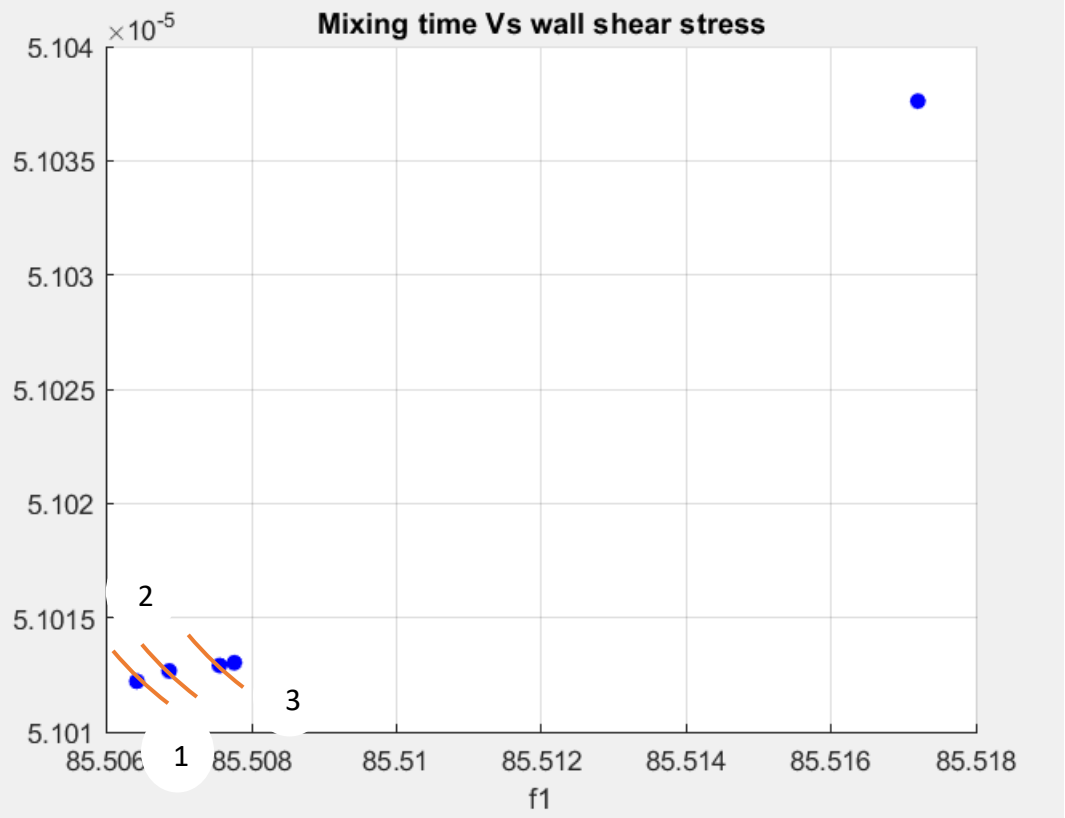

Fig.25 Mixing time vs wall shear stress

Table 3; Comparison of optimum results of all optimization techniques (t_{mix}. Vs τ_{max})

Optimization techniques	Optimum Results				
	t_{mix}. (s)	τ_{max}(pa)	$Q(m^3s^{-1})$	$h(m)$	$R1(m)$
Genetic Algorithm	130	2.7	0.0002	0.0502	0.0036
Particle-swarm optimization	103	0.23	0.0015	0.0312	0.0181
TLBO	118	3	0.0010	0.0302	0.0117
Cuckoo-search optimization	115	0.3	0.0023	0.0203	0.0114

Table 4: Comparison of optimum results of all optimization techniques (t_{mix} vs As)

Optimization techniques	Optimum Results				
	t_{mix}(s)	$As(m^2)$	$Q(m^3s^{-1})$	$h(m)$	$R1(m)$
Genetic Algorithm	95	0.22	0.0001	0.0432	0.0043
Particle-swarm optimization	103	0.22	0.0014	0.0137	0.0432
TLBO	105	0.19	0.0040	0.0123	0.0112
Cuckoo-search optimization	110	0.15	0.0021	0.0112	0.0110

Table 5: Comparison of optimum results of all optimization techniques (As vs τ_{max})

Optimization techniques	Optimum Results				
	As(m^2)	τ_{max}(pa)	*Q(m^3s^{-1})*	*h(m)*	*R1(m)*
Genetic Algorithm	0.05	1.25	0.0013	0.0411	0.0034
Particle-swarm optimization	0.194	4.38	0.0012	0.0312	0.0123
TLBO	0.06	1.6	0.0023	0.0012	0.0121
Cuckoo-search optimization	0.025	0.25	0.0014	0.0023	0.0211

5.5. Optimum Results (For dual gas purging)

5.5.1 Genetic Algorithm

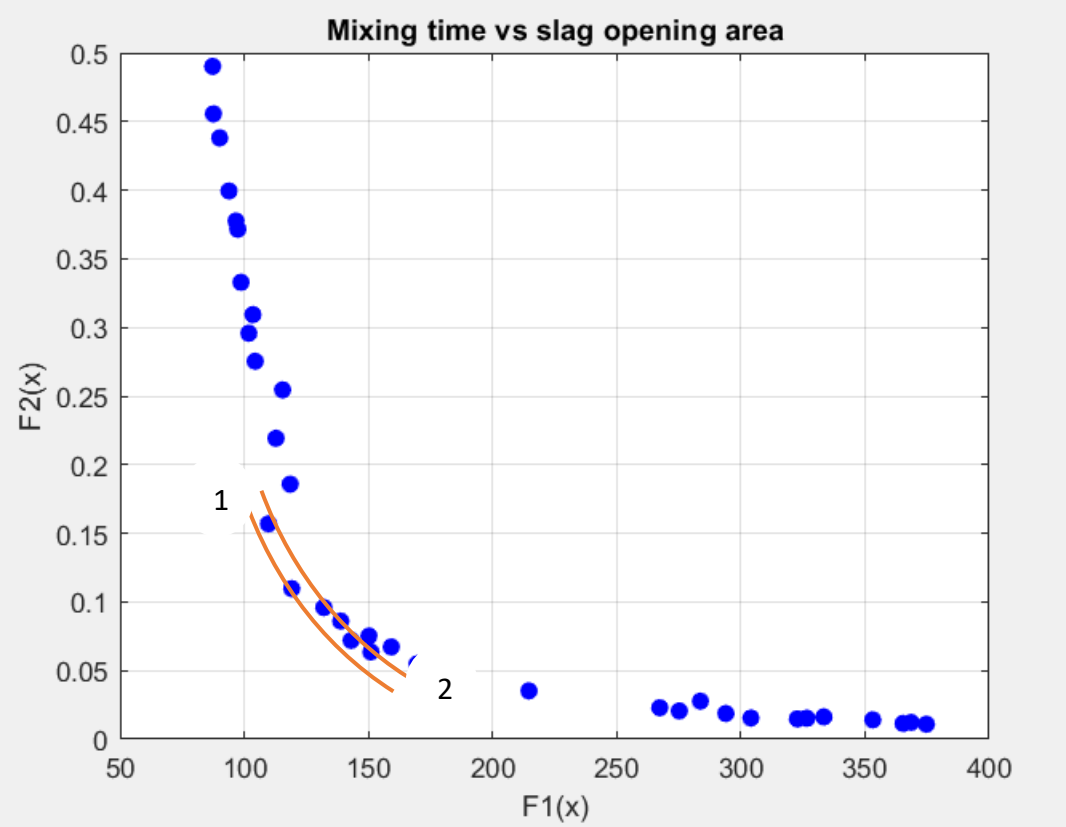

Fig.26 Mixing time vs slag opening area

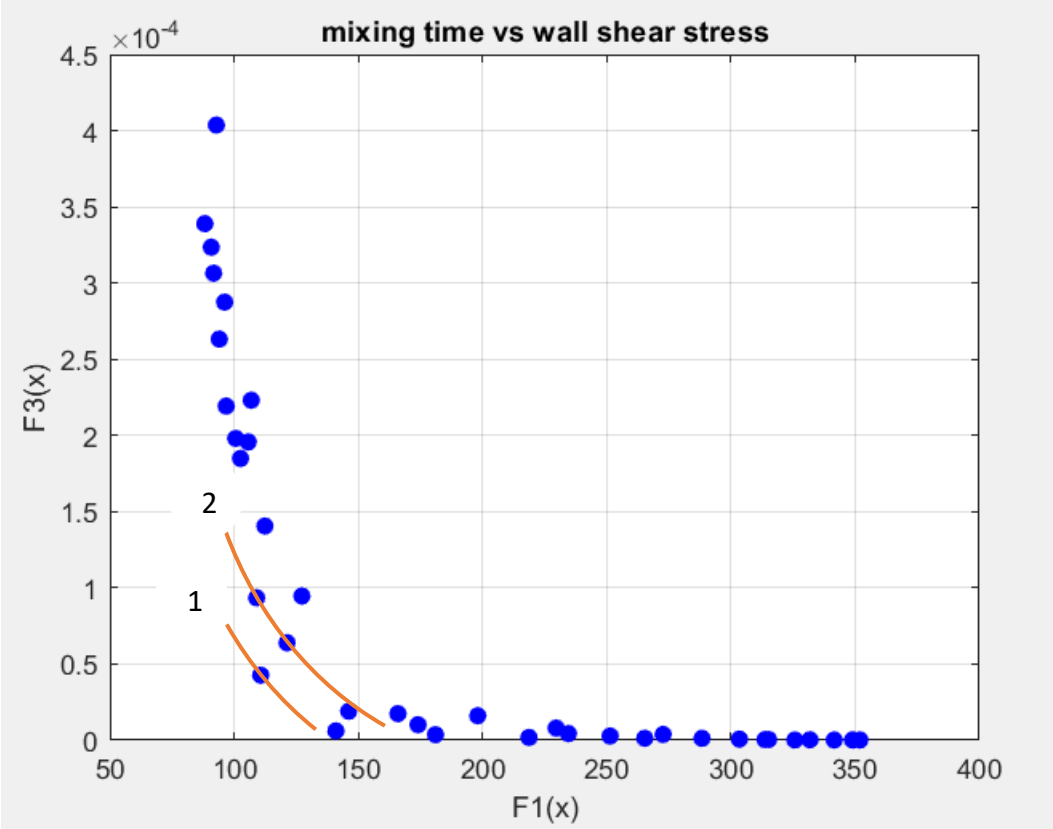

Fig.27 Mixing time vs wall shear stress

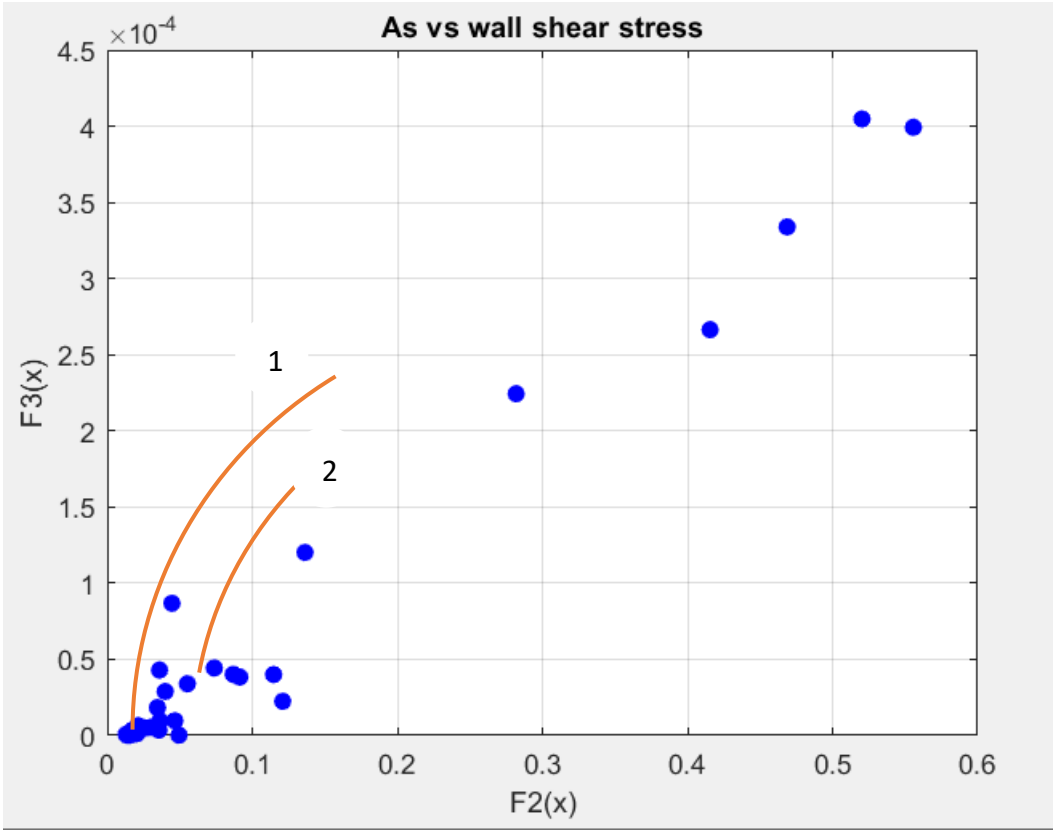

Fig.28 Slag opening area vs wall shear stress

Table 6: Optimal solutions

t_{mix}	τ_{max}	Q	h	R1	R2	R3
88.8520	0.3	0.0020	0.0272	0.2652	0.2997	0.1008
352.2606	0.1	0.0002	0.0960	0.0007	0.1180	0.6029
353.0345	0.3	0.0002	0.0948	0.0007	0.1180	0.6184
92.6916	0.4	0.0020	0.0455	0.3109	0.3134	0.1258
346.0577	0.1	0.0003	0.0918	0.0006	0.1236	0.6309
94.1032	0.3	0.0019	0.0281	0.2626	0.2661	0.1190
312.1546	0.3	0.0003	0.0846	0.0019	0.1437	0.5895
110.7133	0.1	0.0019	0.0313	0.0752	0.1514	0.1876
88.8520	0.3	0.0020	0.0272	0.2652	0.2997	0.1008
99.0650	0.2	0.0020	0.0495	0.1394	0.2854	0.1276
132.5725	0.5	0.0017	0.0233	0.0380	0.0372	0.7604

5.5.2 Cuckoo-search optimization

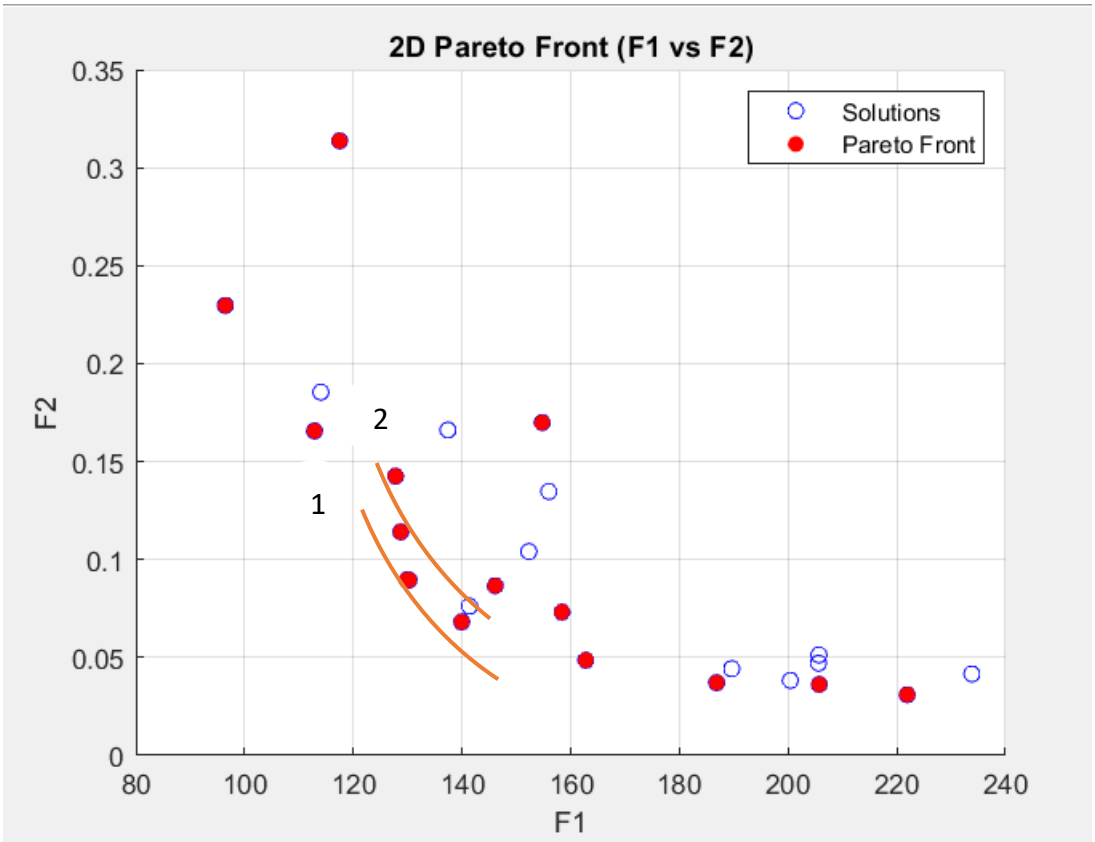

Fig.29 Mixing time vs slag opening area

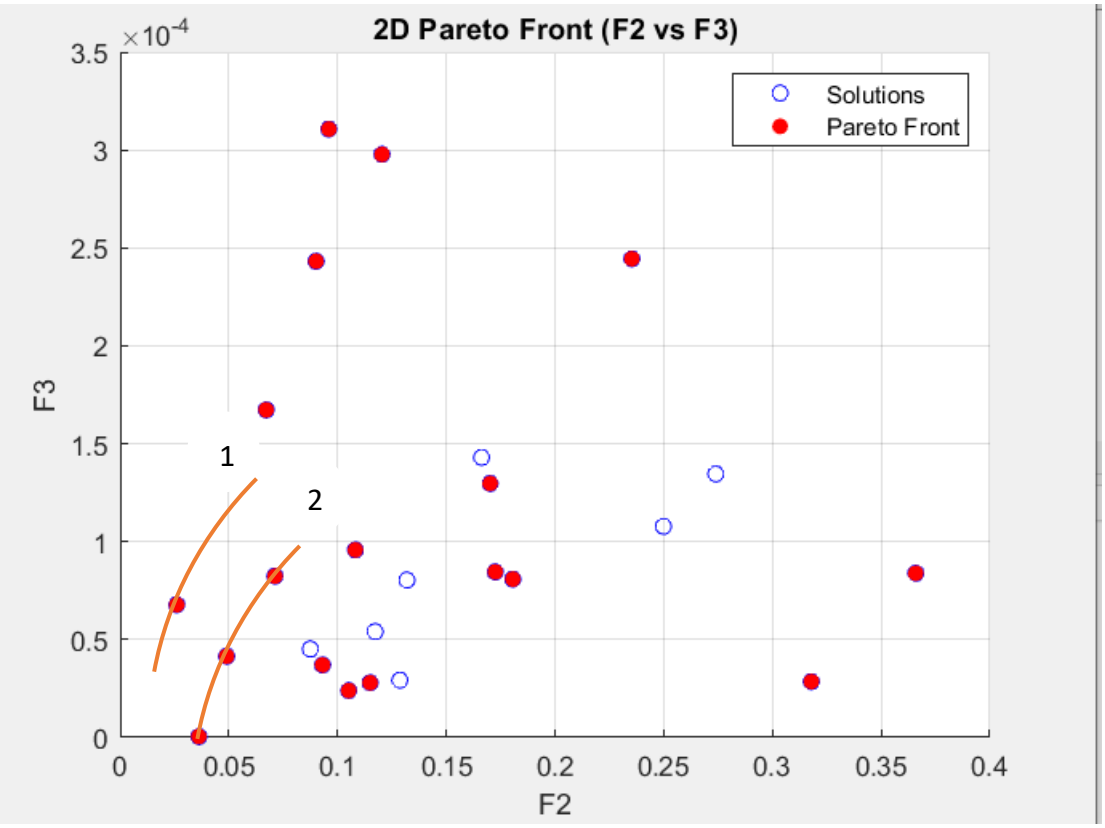

Fig.30 Slag opening area vs wall shear stress

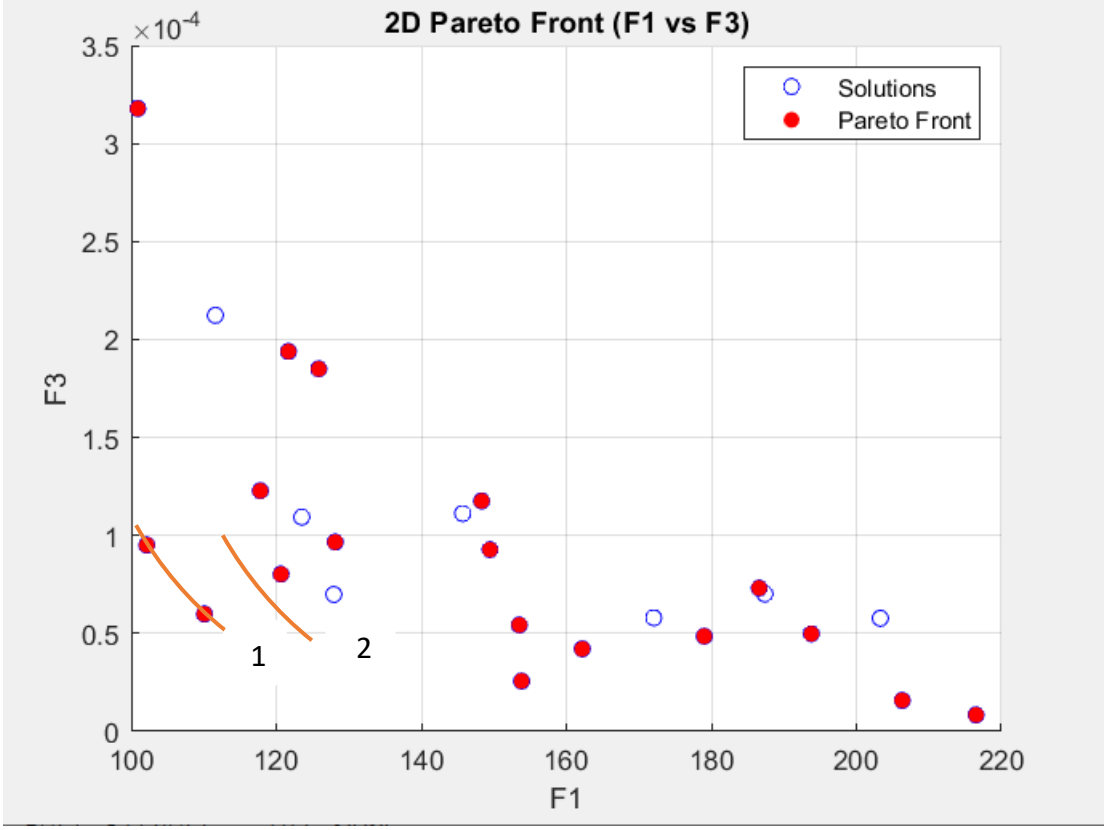

Fig.31 Mixing time vs wall shear stress

5.6 Results and Validation

5.6.1 For single purged ladle (Q= 0.0015 m^3s h=0.0312 R_1=0.0181m from table 3)

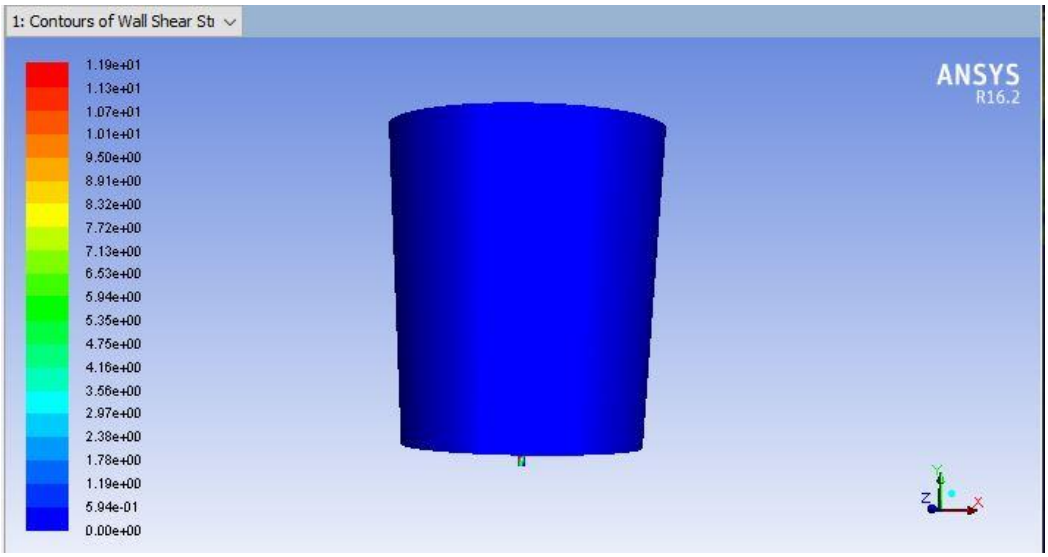

Fig.32 Shear stress distribution in single purged ladle

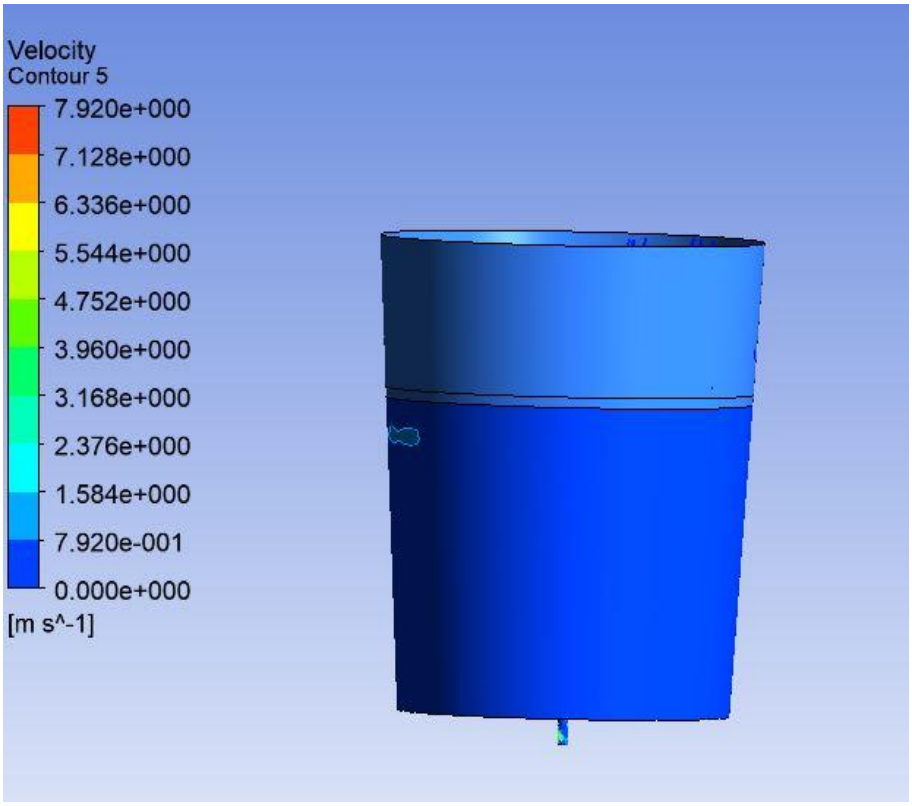

Fig.33 Velocity distribution in single purged ladle

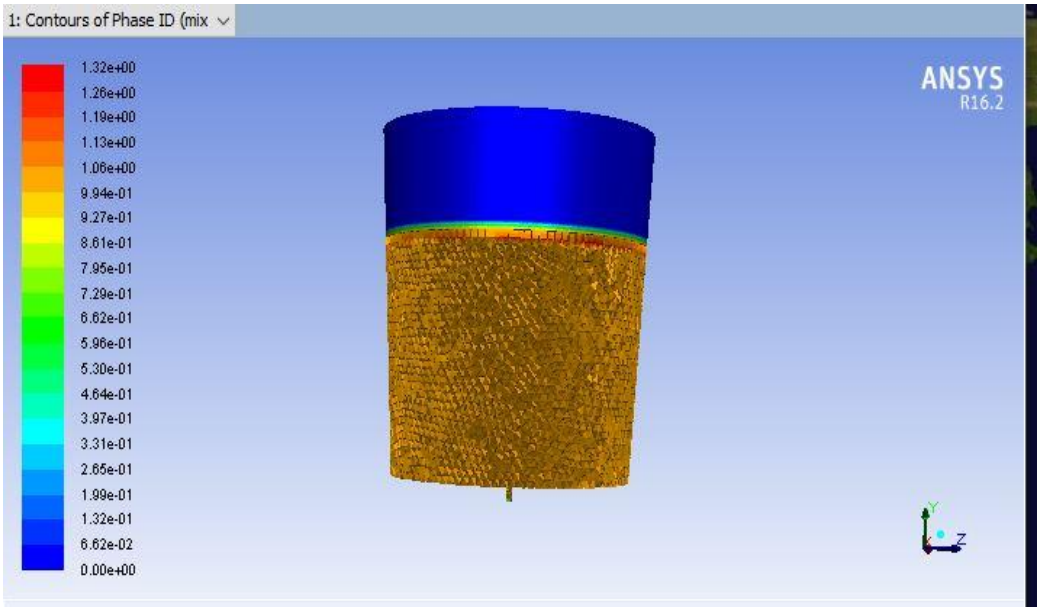

Fig.34 Contour of phase index

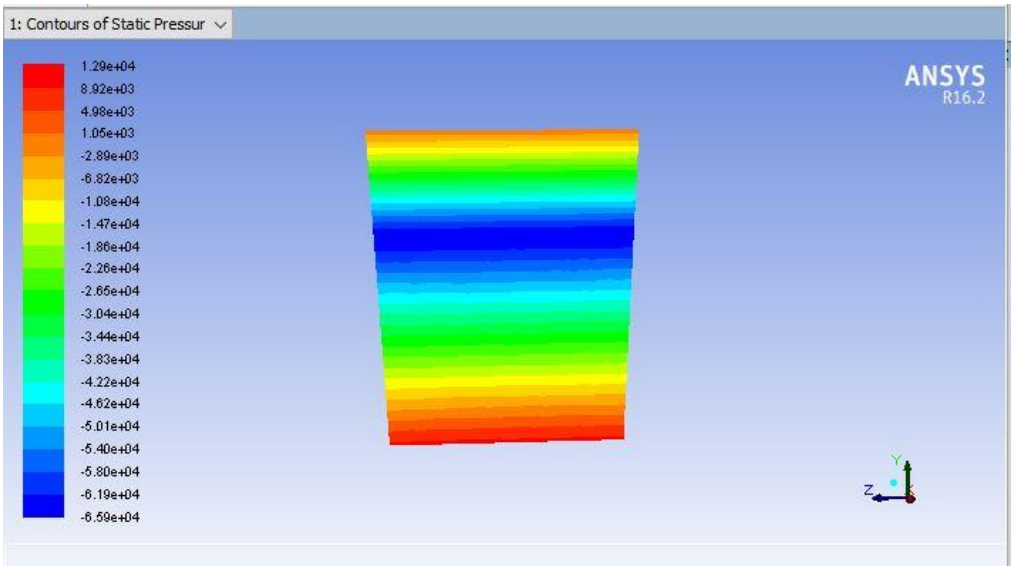

Fig.35 Contour of static pressure in single purged ladle

5.6.2 For Dual Purged ladle (Q=0.0017 h=0.0233 R1=0.0380 R2=0.0370 R3=0.0604)

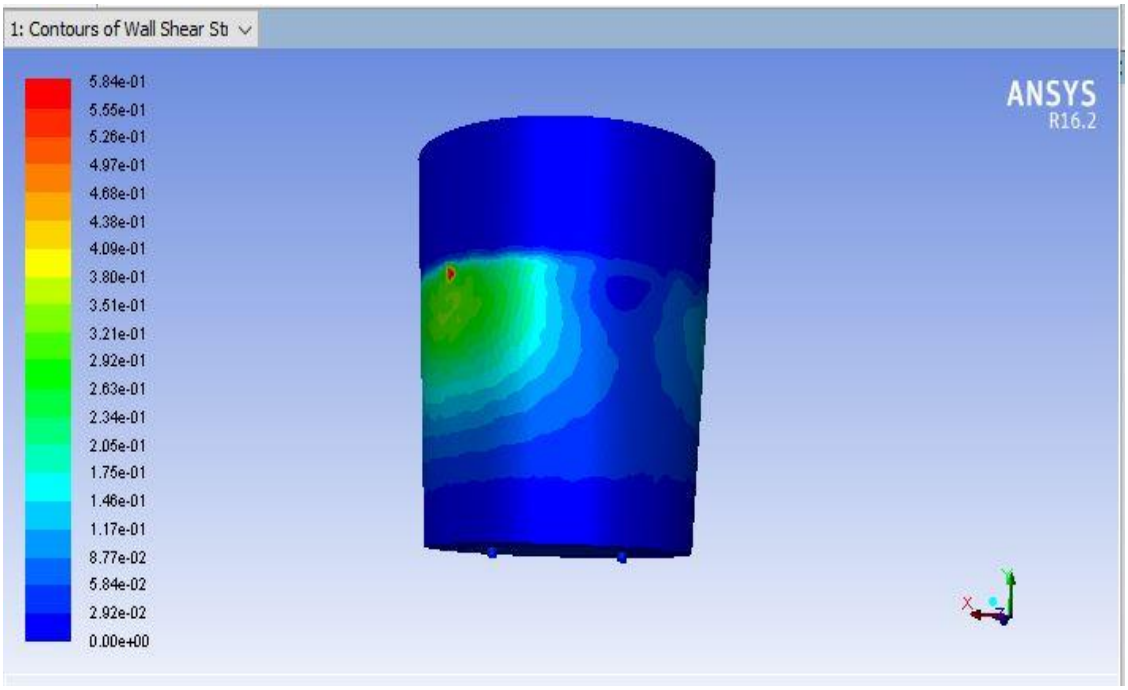

Fig.36 Wall shear stress distribution in dual purged ladle

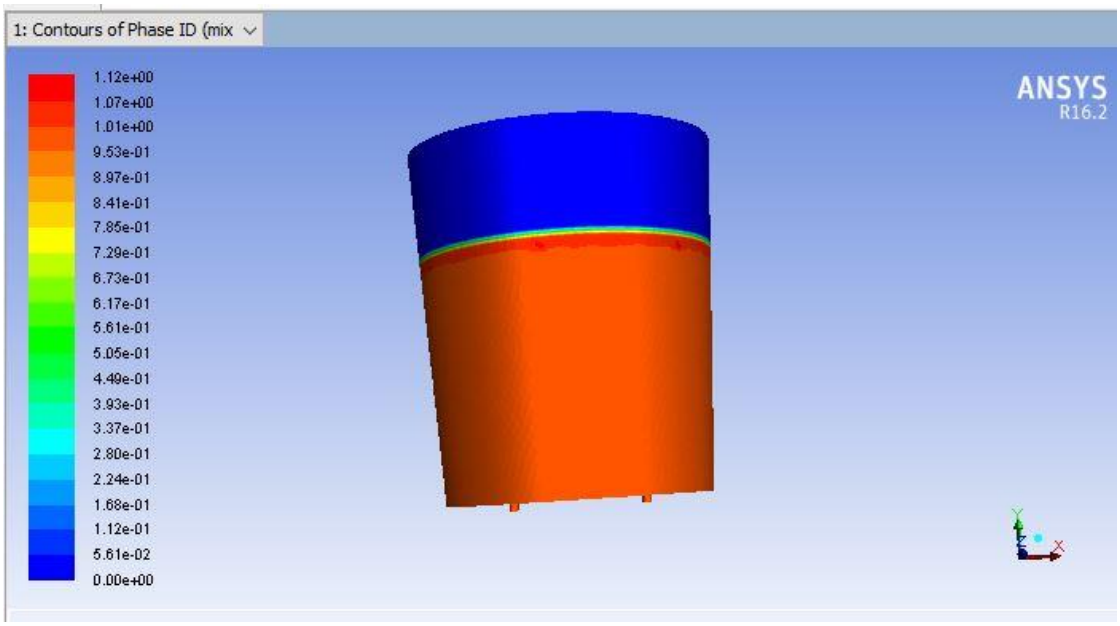

Fig. 37 Contours of phase index in dual purged ladle

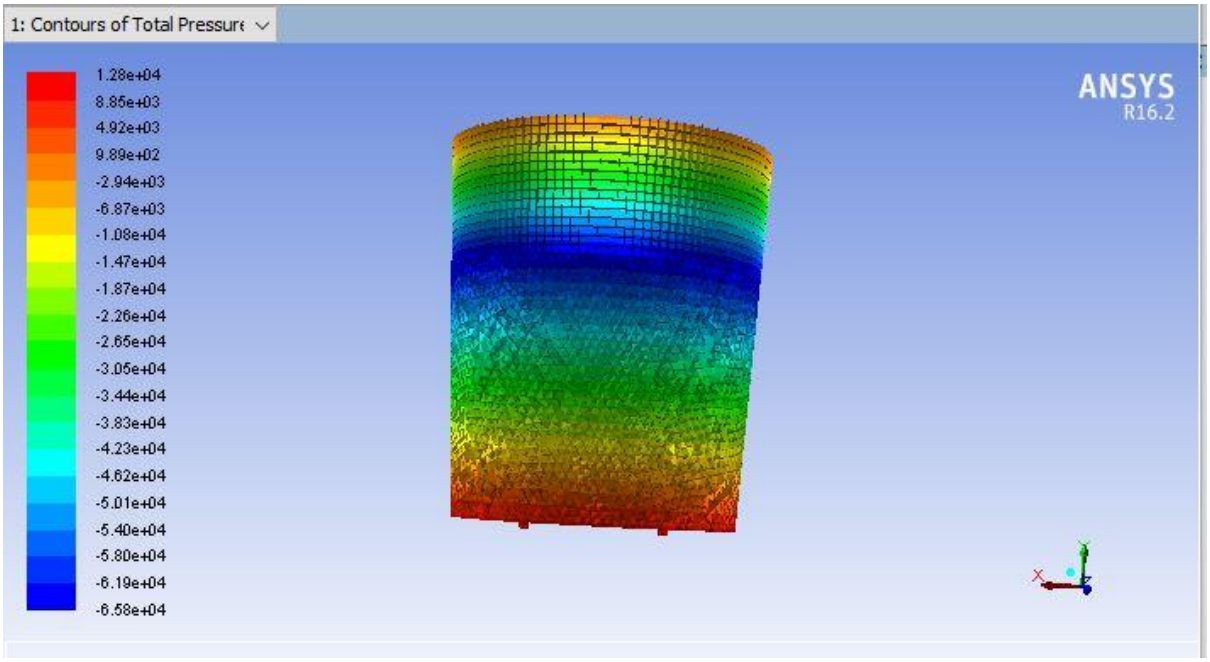

Fig. 38 Contours of total pressure in dual purged ladle

6. Conclusions and Future work

A mathematical model is formulated to predict the mixing time, slag opening area, and wall shear stress in single and dual purged industrial steelmaking ladles is as following-

- For Single purged ladle

$$t_{mix} = 15.48 \times Q^{-0.319} \times h^{0.086} \times R_1^{-0.037}$$

$$A_s = 2.991 \times Q^{0.745} \times h^{-0.882} \times R_1^{0.036}$$

$$\tau_{max} = 0.0014 \times Q^{0.516} \times h^{-0.228} \times R_1^{0.121}$$

- For Dual Purged ladle

$$t_{mix} = 15.96 \times Q^{-0.324} \times h^{0.055} \times R_1^{-0.061} \times R_2^{-0.069} \times R_3^{0.113}$$

$$A_S = 0.566 \times Q^{-0.685} \times h^{-1.061} \times R_1^{0.079} \times R_2^{0.057} \times R_3^{-0.207}$$

$$\tau_{max} = 0.1883 \times Q^{0.7494} \times h^{-0.0194} \times R_1^{0.8548} \times R_2^{0.6572} \times R_3^{-0.0742}$$

Further, Optimization techniques i.e., Genetic algorithm, particle swarm optimization, cuckoo-search optimization and teaching learn based optimization is performed to optimize the ladle objectives functions.

After that comparison is taken place of all optimization techniques and the best optimal solution is achieved as following-

For single purged ladle

t_{mix}. (s)	τ_{max}(pa)	$Q(m^3s^{-1})$	*h(m)*	*R1(m)*
103	0.23	0.0015	0.0312	0.0181

For dual purged ladle

t_{mix}. (s)	τ_{max}(pa)	$Q(m^3s^{-1})$	*h(m)*	*R1(m)*	*R2(m)*	*R3(m)*
132.57	0.50	0.0017	0.0233	0.0380	0.0372	0.0604

Further an analysis is done for achieving the above optimized results and is shown in fig.32 and fig.36

6.1Future work

- In future analysis of mixing time and slag opening area have to perform because if slag opening area is maximum then there will be chance of oxidation in the liquid steel and then quality of the liquid steel will decrease.
- Analysis of slag opening area vs wall shear stress that means due to wall shear stress how much slag opening area is generating because if these two will increase then ladle life and quality of the steel will decrease.

7. References

1. J. Szekely, H. J. Wang and K. M, “Flow pattern velocity and turbulence energy measurements and predictions in a water model of an argon stirred ladle”, *Metall. Mater. Trans. B,* vol. 7, pp. 287−295, June. 1975.

2. O. J. Ilegbusi, J. Szekely, M. Iguchi, H. Takeuchi and Z.-I. Morita, “A Comparison of Experimentally Measured and Theoretically Calculated Velocity Fields in a Water Model of an Argon Stirred Ladle,” *ISIJ Int*., Vol. 33, pp. 474−478, Jan. 1993.

3. Y. Xie and F. Oeters, “Experimental studies on the flow velocity of molten steels in a ladle at centric gas blowing”, *Steel Res*., vol. 63, pp. 93−104, March. 1992.

4. Y. Xie, S. Orsten and F. Oeters, “Behaviour of Bubbles at Gas Blowing into Liquid Wood’s meta”, *ISIJ Int*., vol. 32, pp. 66-75, Sep. 1991.

5. J. L. Xia, T. Ahokainen and L. Holappa, “Modelling of Flows in a Ladle with Gas Stirred Liquid Wood’s Metal”, Proceedings of the Second International Conference on CFD in the *Minerals and Process Industries, CSIRO*, Melbourne, Australia, December 6-8, 1999, pp. 187-192.

6. W. Lou and M. Miaoyong Zhu, “Numerical Simulation of Gas and Liquid Two-Phase Flow in Gas-Stirred Systems Based on the Euler−Euler Approach”, *Metall. Mater. Trans. B*, vol. 44, pp.1251-1263, Oct. 2013.

7. C. G. Mendez, N. Nigro and A. Cardona, “Drag and non-drag influences in numerical simulations of metallurgical ladles”, *J. Mater. Process. Technol*., vol 160, pp. 296−305, June. 2014.

8. H. Türkoğlu and B. Farouk, “Numerical computations of fluid flow and heat transfer in a gas-stirred liquid bath”, *Metall. Mater. Trans. B,* vol. 21 pp. 771−781, June. 1990.

9. M. R. Davidson, “Numerical calculations of two-phase flow in a liquid bath with bottom gas-injection: The central plume”, *Appl. Math. Model*., vol. 14, pp. 67−76, Feb. 1999.

10. J. F. Domgin, P. Gardin and M. Brunet, “Experimental and numerical investigations of gas stirred ladles”, Proceedings of the *Second International Conference on CFD in the Minerals and Process Industries*, Melbourne, Australia, CSIRO, Melbourne, Australia, December 6-8, 1999, pp. 181-186.

11. H-J. Park and W-J. Yang, “Turbulent two-phase mixing in gas-stirred systems for continuous casting applications”, *Numer. Heat Tr. A-Appl*., vol. 31, pp. 493−515, March. 1997.

12. Y. Liu, M. Ersson, H. Liu, P. G. Jönsson and Y. Gan, “A Review of Physical and Numerical Approaches for the Study of Gas Stirring in Ladle Metallurgy”, *Metall. Mater. Trans. B,* vol. 50, pp. 555−577, Feb. 2019.

13. K. Yonezawa and K. Schwerdtfeger, “Spout Eyes Formed by an Emerging Gas Plume at the Surface of a Slag-Covered Metal Melt”, *Metall. Mater. Trans. B,* vol. 30, pp. 411−418, June. 1999.

14. K. Yonezawa and K. Schwerdtfeger, “Height of the Spout of a Gas Plume Discharging from a Metal Melt”, *Metall. Mater. Trans. B*, vol. 30, pp. 655-660, Aug. 1999.

15. K. Yonezawa and K. Schwerdtfeger, “Dynamics of the Spout of Gas Plumes

Discharging from a Melt: Experimental Investigation with a Large-Scale Water Model”, *Metall. Mater. Trans. B*, vol. 31, pp. 461-468, June. 1999.
16. K. Krishnapisharodoy and G. A. Irons, “Modeling of Slag Eye Formation over a Metal Bath Due to Gas Bubbling”, *Metall. Mater. Trans. B,* vol. 37, pp.763−772, Oct. 2006.
17. K. Krishnapisharodoy K and G.A. Irons, “An Extended Model for Slag Eye Size in Ladle Metallurgy”, *ISIJ Int*., vol. 48, pp. 1807−1809, Aug. 2008.
18. L. Wu, P. Valentin and D. Sichen, “Study of Open Eye Formation in an Argon Stirred Ladle”, *Steel Res Int*., vol. 8, pp. 508−515, April. 2010.
19. M. Thunman, S. Eckert, O. Hennig, J. Bkörkvall and Du. Sichen, “Study on the Formation of Open-eye and Slag Entrainment in Gas Stirred Ladle”, *Steel Res Int*., vol. 78, pp. 849−856, June. 2007.
20. A. M. Amaro-Villeda, M. A. Ramirez-Argaez and A. N. Conejo, “Effect of Slag Properties on Mixing Phenomena in Gas Stirred Ladles by Physical Modelling”, *ISIJ Int*., vol. 54, pp. 1−8, Aug. 2014.
21. A. Maruyama and M. Iguchi, “Cold Model Study of Spout Eye Area in the Presence of the Slag Layer Simulated by Low-Density Particles”, *J. JSEM*, vol. 12, pp. 7-10, April. 2012.
22. D. Mazumdar, P. Dhandpani and R. Saravanakumar, “Modelling and Optimization of Gas Stirred Ladle Systems”, *ISIJ Int*., vol. 57, pp. 286−295, Oct. 2017.
23. Z. Liu, L. Li and B. Li, “Modeling of the Gas-Steel-Slag Three-Phase Flow in Ladle Metallurgy: Part 1. Physical Modeling”, *ISIJ Int*., vol. 57, pp.1971-1979, June. 2017.
24. L. Li, Z. Liu, B. Li, H. Matsuura and T. Fumitaka, “Water Model and CFD-PBM Coupled Model of Gas-Liquid-Slag Three-Phase Flow in Ladle Metallurgy”, *ISIJ Int*., vol.55, pp. 1337-1346, Feb. 2015.
25. L. Li, Z. Liu, M. Cao and B. Li, “Large Eddy Simulation of Bubble Flow and Slag Layer Behaviour in Ladle with Discrete Phase Model (DPM)-Volume of Fluid (VOF) Coupled Model”, *JOM*, vol. 67, pp. 1459-1467, June. 2015.
26. L. Li and B. Li, “Investigation of Bubble-Slag Layer Behaviours with Hybrid Eulerian-Lagrangian Modeling and Large Eddy Simulation”, *JOM*, vol. 68, pp. 2160-2169, March. 2016.
27. F. A. Calderon-Hurtado, R. M. Davila, K. Chattopadhyay and S. Garcia-Hernandez, “Fluid Flow Turbulence in the Proximities of the Metal-Slag Interface in Ladle Stirring Operations”, *Metals*, vol. 9, pp. 1-17, Feb. 2019.
28. W. Liu, H. Tang, S. Yang, M. Wang, J. Li, Q. Liu and J. Liu, “Numerical Simulation of Slag Eye Formation and Slag Entrapment in a Bottom-Blown Argon-Stirred Ladle”, *Metall. Mater. Trans. B*, vol. 49, pp. 2681-2691, Oct. 2018.
29. L. Li, B. Li and Z. Liu, “Modeling of Gas-Steel-Slag Three-Phase Flow in Ladle Metallurgy: Part II. Multi-scale Mathematical Model”, *ISIJ Int*., vol. 57, pp.1980−1989, Oct. 2017.
30. N.-N. Lv, L.-S. Wu, H.-C. Wang, Y.-Y. Dong and C. Su, “Size Analysis of Slag Eye Formed by Gas Blowing in Ladle Refining”, *J. Iron Steel Res. Int*., vol. 24, pp. 243-250, March. 2017.

31. D. Mazumdar and R. I. L. Guthrie, “On Mathematical Models and Numerical Solutions of Gas Stirred Ladle Systems”, *Appl. Math. Model*., vol. 17, pp. 255-262, May. 1993.
32. D. Mazumdar D and R. I. L. Guthrie, “Numerical Computation of Flow and Mixing in Ladle Metallurgy Steelmaking Operations (C.A.S method)”, *Appl. Math. Model*., vol.10, pp. 25-32, Feb. 1986.
33. D. Mazumdar D and R. I. L. Guthrie, “The Physical and Mathematical Modelling of Gas Stirred Ladle Systems”, *ISIJ Int*., vol. 35, pp.1−20, Sep. 1995.
34. D. Mazumdar, R. Yadhav and B. Mahato, “Transient Flow and Mixing in Steelmaking Ladles during the Initial Period of Gas Stirring”, *ISIJ Int*., vol. 42, pp.106−108, Sep.2002.
35. D. Mazumdar and J. W. Evans, “A Model for Estimating Exposed Plume Eye Area in Steel Refining Ladles Covered with Thin Slag”, *Metall. Mater. Trans. B*, vol. 35, pp. 400-404, April. 2004.
36. J. Mandal, S. Patil, M. Madan and D. Mazumdar, “Mixing Time and Correlation for Ladles Stirred with Dual Plugs”, *Metall. Mater. Trans. B*, vol. 36, pp. 479-487, Aug. 2005.
37. M. Peranadhanthan and D. Mazumdhar, “Modeling of Slag Eye in Argon Stirred Ladles”, *ISIJ Int*., vol. 50, pp. 1622-1631, Aug. 2010.
38. M. Madan, D. Satish and D. Mazumdar, “Modeling of Mixing in Ladles Fitted with Dual Plugs”, *ISIJ Int*., vol. 45, pp. 677-685, Feb. 2005.
39. S. P. Patil, D. Satish, M. Peranandhanathan and D. Mazumdar, “Mixing Models for Slag Covered, Argon Stirred Ladles”, *ISIJ Int*., vol. 50, pp.1117-1124, June. 2010.
40. Subagyo, G. A. Brooks and G. A. Irons, “Spout Eyes Area Correlation in Ladle Metallurgy”, *ISIJ Int*., vol 43, pp. 262-263, Oct. 2003.
41. D. C. Guo, L. Gu and G. A. Irons, “Developments in Modelling of Gas Injection and Slag Foaming”, *Appl. Math. Model*., vol. 26, pp. 263-280, April. 2002.
42. P. Valentin, C. Bruch, Y. Kyrylenko, H. Köchner and C. Dannert, “Influence of the Stirring Gas in a 170-t Ladle on Mixing Phenomena-Formation and On-line Control of Open-Eye at an Industrial LD Steel Plant”, *Steel Res Int*., vol. 80, pp. 552−558, March. 2009.
43. H. Liu, Z. Qi and M. Xu, “Numerical Simulation of Fluid Flow and Interfacial Behaviour in Three-phase Argon-Stirred Ladles with One Plug and Dual Plugs”, *Steel Res Int*., vol. 82, pp. 440−458, Nov. 2011.
44. B. Li, H. Yin, C. Q. Zhou and F. Tsukihashi, “Modeling of Three-phase Flows and Behaviour of Slag/Steel/Interface in an Argon Gas Stirred Ladle”, *ISIJ Int*., vol. 48, pp. 1704-1711, Sep. 2008.
45. U. Singh, R. Anapagaddi, S. Managal, K. A. Padmanabhan and A. K. Singh, “Multiphase Modeling of Bottom-Stirred Ladle for Prediction of Slag-Steel Interface and Estimation of Desulfurization Behaviour”, *Metall. Mater. Trans. B*, vol. 47, pp. 1804-1816, June. 2016.
46. H. Gonzalez, J. A. Ramos-Baderas, E. Torres-Alonso, G. Solorio-Diaz, C. A. Hernandez-Bocanegra, “Multiphase Modeling of Fluid Dynamic in Ladle Steel

Operations Under Non-isothermal conditions”, *J. Iron Steel Res. Int*., vol. 24, pp. 888-900, Sep. 2017.
47. S. W. P. Cloete, J. J. Eksteen and S. M. Bradshaw, “A Mathematical Modelling Study of Fluid Flow and Mixing in Full-Scale Gas-Stirred Ladles”, *Prog. Comput. Fluid Dyn*., vol. 9, pp. 345-356, A pril. 2009.
48. S. W. P. Cloete, J. J. Eksteen and S. M. Bradshaw, “A Numerical Modelling Investigation into Design Variables Influencing Mixing Efficiency in Full Scale Gas Stirred Ladles”, *Miner. Eng*., vol. 46-47, pp. 16-24, May. 2013.
49. Q. Cao and L. Nastac, “Mathematical Investigation of Fluid Flow, Mass Transfer, and Slag-steel Interfacial Behaviour in Gas-stirred Ladles”, *Metall. Mater. Trans. B*, vol.49, pp. 1388-1404, June. 2018.
50. Q. Cao and L. Nastac, “Numerical Modelling of the Transport and Removal of Inclusions in an Industrial Gas-stirred Ladle”, *Ironmaking & Steelmaking*, vol. 45, pp. 984-991, Jan. 2018.
51. T. Palovaara, V.-V. Visuri and T. Fabritius, ” Physical modelling of gas injection in a ladle”, *Proceedings of the 7th International Congress on Science and Technology of Steelmaking*, Associazione Italiana di Metallurgia, Venice, Italy, 2018.
52. K. Michalek, K. Gryc and J. Moravka, “Physical Modelling of Bath Homogenization in Argon Stirred Ladle”, *Metalurgija*, vol. 48, pp. 215-218, Oct. 2009.
53. S. Joo and R. I. L. Guthrie, “Modeling Flows and Mixing in Steelmaking Ladles Designed for Single-and Dual-plug Bubbling Operations”, *Metall. Mater. Trans. B*, vol. 23, pp. 765-778, March.1992.
54. M. S. C. Terrazas and A. Conejo, “Effect of Nozzle Diameter on Mixing Time during Bottom-Gas Injection in Metallurgical Ladles”, *Metall. Mater. Trans. B*, vol. 46, pp. 711-718, April. 2015.
55. A. N. Conejo, S. Kitamura, N. Maruoka and S.-J Kim, “Effects of Top Layer, Nozzle Arrangement, and gas Flow Rate on Mixing Time in Agitated Ladles by Bottom Gas Injection”, *Metall. Mater. Trans. B*, vol. 44, pp. 914-923. Aug. 2013.
56. S.-M. Pan, J.-D. Chaing and W.-S.Hwang, “Effects of Gas Injection Condition on Mixing Efficiency in the Ladle Refining Process”, *JMEPEG*, vol. 6, pp. 113-117. Feb. 1997.
57. J. Aoki, B. G. Thomas, J. Peter and K. D. Peaslee, “Experimental and Theoretical of Mixing in a Bottom Gas-Stirred Ladle”, *AISTech Proceedings*, Nashville, United States of America, September 15-17, 2004, pp. 1045-1056.
58. Q. Cao Q and L. Nastac, “Mathematical Modeling of the Multiphase Flow and Mixing Phenomena in a Gas-Stirred Ladle: The Effect of Bubble Expansion”, *JOM*, vol. 70, pp.2071-2081, June. 2018.
59. W. Lou W and M. Zhu, “Numerical Simulations of Inclusion Behaviour and Mixing Phenomena in Gas-stirred Ladles with Different Arrangement of Tuyeres”, *ISIJ Int*., vol. 54, pp. 9-18, Aug. 2014.
60. M Iguchi, IIegbusi, and J Olusegun. Modeling Multiphase Materials Processes. Springer-Verlag New York, 2011.
61. Baokuan Li, Hongbin Yin, Chenn Q Zhou & Fumitaka Tsukihashi.

Modeling of Three phase Flows and Behavior of Slag Steel Interface in an Argon Gas Stirred Ladle. ISIJ Int., 48 (2008) 1704–1711.
62. P Mavros. Flow visualization in stirred vessels: A review of experimental techniques. Chem. Eng. Res. & Des., 79 (2001) 113–127.
63. Krishnakumar Krishnapisharody, N B Ballal, P K Sinha, M K Sardar & K N Jha. Water Model Experiments on Mixing Phenomena in a VOD Ladle. ISIJ Int., 39 (1999) 419–425.
64. M Zhu, T Inomoto, I Sawada & T Hsiao. Fluid Flow and Mixing Phenomena in the Ladle Stirred by Argon through Multi-Tuyere. ISIJ Int., 35 (1995) 472–479.
65. Marco A Ramirez-Argaez. Numerical simulation of fluid flow and mixing in gas-stirred ladles. Mat. & Manuf. Proc., 23 (2007) 59–68.
66. Marek Warzecha, Jan Jowsa, Piotr Warzecha & Herbert Pfeifer. Numerical and Experimental Investigations of Steel Mixing Time in a 130-T Ladle. Steel Res. Int., 79 (2008) 852–860.
67. A. Tripathi, J.K. Saha, J.B. Singh, S.K. Ajmani. Numerical simulation of heat transfer phenomenon in steel making ladle. ISIJ Int., 52 (2012), 1591–1600.

Appendix 1(MATLAB code)

```
% Define the objective functions
f1 = @(x,y,z) 15.48 * x.^(-0.319) .* y.^(0.086) .* z.^(-0.037);
f2 = @(x,y,z) 2.991 * x.^(0.745) .* y.^(-0.882) .* z.^(0.036);
f3 = @(x,y,z) 0.0014 * x.^(0.516) .* y.^(0.0228) .* z.^(0.021);

% Combine objective functions into a multi-objective function handle
multiObjFunc = @(x) [f1(x(1), x(2), x(3)), f2(x(1), x(2), x(3)), f3(x(1),
x(2), x(3))];

% Define the bounds for the decision variables
lb = [2.02e-4, 0.025, 3.25e-4]; % Lower bounds for x, y, z
ub = [20.20e-4, 0.10, 0.325];   % Upper bounds for x, y, z

% Define options for the multi-objective optimization
options = optimoptions('paretosearch', 'Display', 'iter');

% Perform multi-objective optimization using paretosearch (constrained)
[x, fval, exitflag, output] = paretosearch(multiObjFunc, 3, [], [], [], [],
lb, ub, []);

% Display the results
disp('Optimal Solution (x, y, z):');
disp(x);
disp('Objective Function Values (f1, f2, f3):');
disp(fval);
```

Appendix 2

```
% Define the objective functions
F1 = @(x) 15.96 * x(1)^-0.324 * x(2)^0.055 * x(3)^-0.061 * x(4)^-0.069 *
x(5)^0.113;
F2 = @(x) 0.566 * x(1)^0.685 * x(2)^-1.061 * x(3)^0.079 * x(4)^0.057 *
x(5)^-0.207;
F3 = @(x) 0.1883 * x(1)^0.7494 * x(2)^-0.0194 * x(3)^0.8548 * x(4)^0.6572 *
x(5)^-0.0742;

% Combine the objective functions into a single function handle
objectiveFunction = @(x) [F1(x), F2(x), F3(x)];

% Define the bounds for the variables
lb = [2.02e-4, 0.025, 3.25e-4, 9.60e-2, 9.56e-2];
ub = [20.20e-4, 0.10, 0.325, 0.325, 0.650];

% Set options for the genetic algorithm
 options = optimoptions('gamultiobj', ...
'PopulationSize', 100, ...
'MaxGenerations', 500, ...
'Display', 'iter', ...
'UseParallel', true);

% Run the genetic algorithm
[x, fval] = gamultiobj(objectiveFunction, 5, [], [], [], [], lb, ub,
options);

% Display the results
disp('Optimal solution:')
disp(x)
disp('Objective function values at the optimal solution:')
disp(fval)
% Plotting the 2D Pareto front
figure;
plot(fval(:,1), fval(:,3), 'bo', 'MarkerSize', 6, 'MarkerFaceColor', 'b');
xlabel('F1(x)');
ylabel('F3(x)');
title('2D Pareto Front between F1 and F3');
grid on;
```